Technical Report
TR-19-18
April 2019

Subglacial block removal – a preliminary analysis of driving and resisting forces under different glaciological scenarios

Maarten Krabbendam
Adrian M Hall

SVENSK KÄRNBRÄNSLEHANTERING AB

SWEDISH NUCLEAR FUEL
AND WASTE MANAGEMENT CO

Box 3091, SE-169 03 Solna
Phone +46 8 459 84 00
skb.se

SVENSK KÄRNBRÄNSLEHANTERING

ISSN 1404-0344
SKB TR-19-18
ID 1859556
April 2019

Subglacial block removal – a preliminary analysis of driving and resisting forces under different glaciological scenarios

Maarten Krabbendam
British Geological Survey, Lyell Centre, Edinburgh

Adrian M Hall
Department of Physical Geography, Stockholm University

Keywords: Block removal, Glacial erosion, Water pressure, Ice thickness, Hard-bed, Ice flow.

Preface

The following report describes a theoretical analysis of glacial erosion, or more specifically of the forces required for the removal of upstanding rock blocks by sliding of ice at the base of an ice sheet under four different glacial scenarios.

The study was initiated by Maarten Krabbendam (British Geological Survey, BGS), and written by Maarten Krabbendam (BGS) and Adrian Hall (Stockholm University). The study constitutes a contribution to the larger SKB project on glacial erosion and bedrock surface exposure age and stability in Forsmark.

The report manuscript was reviewed by Joel Harper (University of Montana) and Jens-Ove Näslund (SKB). An internal BGS review was made by Andrew Finlayson.

The results will be used, together with other scientific information, for constructing future climate scenarios for SKB:s work on assessing the long-term safety of the nuclear waste repositories in Sweden.

Stockholm, February 2018

Jens-Ove Näslund
Research coordinator Climate Programme SKB

Abstract

In this report, we present a preliminary analysis of the forces required for the removal of upstanding rock blocks, such as tors and cnocs, by sliding ice at the base of an ice sheet. We study the driving and resisting forces, mainly as a function of block size in the 1–15 m range. We model block removal in four glacial scenarios: i) cold-based ice; ii) warm-based ice with a thin layer of temperate ice; iii) warm-based ice with a thick layer of temperate ice; and iv) an ice marginal freeze-on scenario. Each scenario has different driving and resisting forces, dependent on ice thickness, ice flow velocities and basal shear stress. The results of the preliminary analysis suggest the following. Block removal is unlikely to occur under cold-based ice. Under warm-based conditions, block removal is strongly dependent on ice velocity and ice viscosity: if blocks are removed by viscous drag, there is a strong sorting effect with smaller blocks being removed and large blocks remaining. In general, the results suggest that block removal is more likely under thin ice than under thick ice. In the ice-marginal freeze-on scenario, block removal is very likely, although it is uncertain whether this scenario is (or was) common in nature. The effect of block shape and streamlining is strong under warm-based sliding: non-cubic flat 'slabs', elongate blocks, or blocks with a sloping lee side are more likely to remain compared to more cubic block shapes. However, if block removal occurs in the freeze-on scenario, the block shape has little effect, and more cubic blocks have a similar probability of removal as streamlined blocks. A major uncertainty of this analysis is whether the viscous drag forces can be modelled by Stoke's Law – it is recommended that in future modelling a more general drag law is used for viscous drag forces.

Sammanfattning

Studien utgör en preliminär analys av de krafter som behövs för att förflytta uppstickande block, som tex tor-former och små bergkullar, genom glidning av is vid botten av en inlandsis. Vi studerade drivande och resistiva krafter i huvudsak som funktion av block i storleksordningen 1–15 m. Vi modellerade förflyttning av block för fyra glaciala scenarier: i) kallbottnad inlandsis, ii) varmbottnad inlandsis med ett tunt lager av ovanliggande tempererad is, iii) varmbottnad inlandsis med ett tjockt lager av ovanliggande tempererad is, och iv) ett scenario med frontnära anfrysning. Var och ett av scenarierna har olika drivande och resistiva krafter beroende på istjocklek, isrörelsehastighet och skjuvspänning vid isens botten. Följande tentativa slutsatser kan dras från studien. Det är osannolikt att förflyttning av block sker om isen är kallbottnad. Om isen är varmbottnad är förflyttning av block starkt beroende av isrörelsehastigheten och isens viskositet: om block flyttas genom viskösa dragkrafter sker en tydlig sortering där mindre block flyttas medan större block inte gör det. Resultaten visar generellt att förflyttning av block är mer sannolik att inträffa om ovanliggande is är tunn än om den är tjock. I scenariot med frontnära anfrysning är det mycket sannolikt att förflyttning av block sker, men det är oklart hur pass vanligt eller ovanligt detta scenario är, eller har varit, i naturen. Effekten av blockens form är tydlig vid varmbottnade förhållanden med bottenglidning: icke-kubiska platta block, avlånga block, eller block med en sluttande distalsida är mindre sannolika att flyttas jämfört med mer kubiskt formade block. Om förflyttning av block sker i scenariot med frontnära anfrysning har dock blockens form mindre betydelse, och mer kubiska block har samma sannolikhet att flyttas som strömlinjeformade block. En stor osäkerhet i denna studie är om viskösa dragkrafter kan modelleras med Stoke's lag. För framtida liknande studier rekommenderas därför användning av en mer generell lag för viskösa dragkrafter.

Contents

1 Introduction

Abrasion and plucking (quarrying) are generally seen as the main mechanisms of subglacial erosion (e.g. Glasser and Bennett 2004). During the Pleistocene glaciations, abrasion and plucking operated beneath successive ice sheets to produce a roughened bed topography of small hills (cnocs), basins and valleys that is characteristic of glaciated lowlands developed on fractured Precambrian gneiss bedrock (e.g. Rastas and Seppälä 1981, Krabbendam and Bradwell 2014). However, the removal of upstanding rock blocks offers another possible mechanism of glacial erosion. Removal of large blocks from tors is known to have occurred in at least the first stages of glacial erosion (e.g. Hall and Phillips 2006). Such a mechanism may potentially be relevant for the erosion of small rock blocks or hills under more advanced glacial erosion and is therefore relevant for a first order analysis of glacial erosion beneath an ice sheet over a glacial cycle.

Here we focus on the small blocks or hills (tors, cnocs) that protrude into the base of the ice sheet. The process of block removal is mechanically different from plucking, mainly because an upstanding block is exposed to a direct pushing force by ice. In this report we analyse the balance of forces required to move a block of bedrock at the bed of an ice sheet, and the glaciological conditions under which these forces may occur.

The study is coupled to the Forsmark site in south-central Sweden, i.e. the site selected by Swedish Nuclear Fuel and Waste Management Company (SKB) for the planned geological repository for spent nuclear fuel. In the assessment of long-term repository safety, which covers a time span of up to one million years, the question of future denudation, including glacial erosion, is of importance (e.g. SKB 2010).

On the shield lowlands in the Forsmark area, relief is low, in part because Pleistocene glacial erosion across Uppland has not greatly modified the exhumed sub-Cambrian peneplain (Beckholmen and Tirén 2009, Lidmar-Bergström et al. 2012, Hall et al. 2019). A nested hierarchy of rock blocks (cnocs and roches moutonnées) exists (Figure 1-1 A and B), but no small, isolated rock hills (tors) are seen. Individual rock blocks show low profiles with lengths of 10–250 m. Smooth, abraded rock surfaces, as well as lateral and lee-side cliffs, occur widely. They indicate the operation of abrasion and plucking but it is unknown to what extent rock block removal may have operated in such subdued terrain. In the Cairngorm mountains in Scotland, rock blocks are seen as prominent tors up to 20 m high but the high plateau lacks clear glacial bedforms, such as cnocs. Glacial erosion has locally removed and transported large blocks from tors and demolished entire tors to leave stumps and plinths (Hall and Phillips 2006) (Figure 1-1 C and D). The widespread occurrence of erratics shows that there is no question that metre-sized blocks can be moved by ice. On the other hand, the survival of non-glacial tors in areas in Scotland and Sweden known to have been glaciated (e.g. Hättestrand and Stroeven 2002, Hall and Glasser 2003) demonstrates that there are circumstances under which upstanding blocks are not moved by ice. This is generally regarded as a result of non-erosive, cold-based ice (e.g. Rapp 1996, Kleman et al. 1997, Hättestrand and Stroeven 2002), and this is one of the scenarios that is tested in the present study.

We simplify the problem by considering the tors or cnocs as single, fracture-bounded rock blocks, ignoring the effects of rounding, or internal fractures within a tor. In essence, the problem is the balance between the resisting force F_{rx} of the block in question versus the driving force F_{dx} exerted by the ice onto the block (Figure 1-2). If the driving force is greater than the resisting force, block removal will occur; conversely, if the resisting force exceeds the driving force then the block stays in place. Intuitively, one would expect that larger blocks are more difficult to move than smaller blocks: the physical basis of this is that the resisting force may rise faster with increasing block size than the driving force. However, as we shall see, this may not be the case, depending on the glaciological scenario.

The focus on this report is the conditions at the basal ice-bed interface. The situation at the actual front of a glacier or ice sheet during a glacial advance, i.e. where push moraines and similar ice-marginal deposits form, falls outside the scope of this report, as the physics and geomorphological constraints are very different.

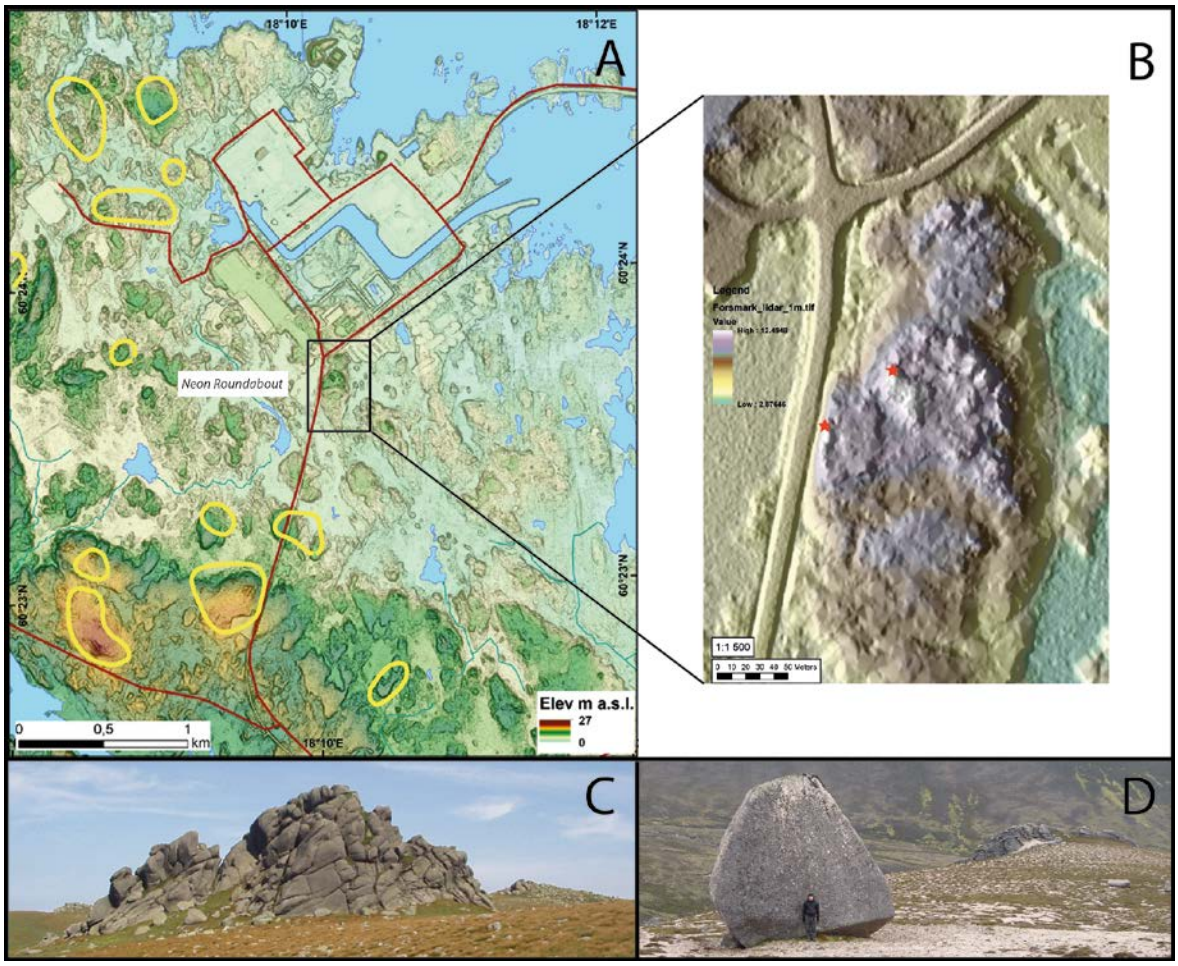

Figure 1-1. *Examples of upstanding rock blocks. (A) Digital Elevation Model (DEM) of the Forsmark area. Note the nested hierarchy of rock hills with A-axis lengths of 25–250 m standing 5–15 m above surrounding fracture-bounded depressions. (B) DEM derived from 1 m resolution LiDAR data for Neon Roundabout, a hill marked by a box on Figure 1-1 A. The hill mass stands up to 10 m above its surroundings and carry many low roches moutonnées with A-axis lengths of 10–20 m. Red stars are sample locations for the cosmogenic dating – reported elsewhere. (C) The tor Clach Choutsaich on Ben Avon at 1 119 m a.s.l. in the eastern Cairngorm Mountains, Scotland. The granite tor has a long axis length of 80 m and a height of 20 m. The tor form lacks evidence of glacial modification beneath successive ice sheets covering the Cairngorm plateau. (D). A 7 m high, cuboidal, glacially-transported tor block at 800 m a.s.l. on the eastern flank of Ben Avon.*

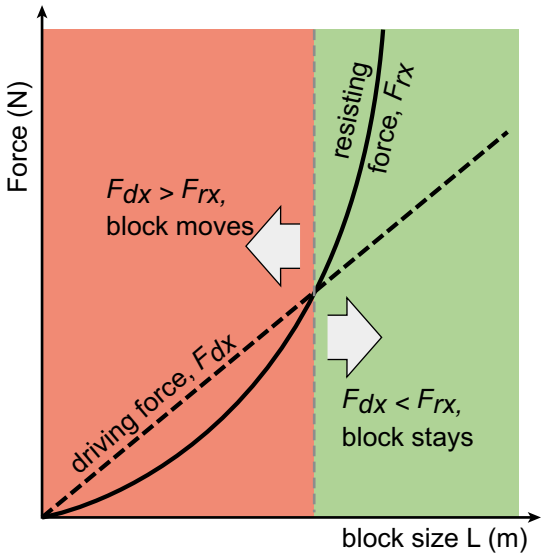

Figure 1-2. *Driving force and resisting force plotted against block size. If the driving force (dotted line) exceeds the resisting force (solid line), a block will move (red field).*

2 Glaciological conditions throughout a glacial cycle

2.1 Scenarios during a glacial cycle

Throughout a glacial cycle, as an ice sheet grows and shrinks, different glaciological conditions occur in a particular place at its bed (e.g. Kleman 1994, Kleman et al. 2008). In the present study, these are regarded as different modelling scenarios: in effect, a set of plausible glaciological conditions at a particular place and time during a glacial cycle. Thus, one location may experience a phase of cold-based ice, where the ice is frozen onto its bed, and later a warm-based phase, where the ice-bed interface is thawed with free water occurring as a thin water film or in small channel networks. Some locations may have a thick layer of temperate ice at the base; elsewhere this layer may be thin. Some locations may experience a phase of fast-flowing ice-stream conditions. At the end of the glaciation, under certain circumstances, the toe of the ice sheet may freeze on its base. Each of these scenarios implies different conditions for both the resisting forces and the driving forces experienced by upstanding blocks. The main parameters of importance are ice temperature, ice viscosity, basal sliding velocity and the subglacial hydrological regime (Figure 2-1). Although we use generic scenarios (see Figure 2-1 lower panel), we use parameter values based on measurements from West Greenland where possible, e.g. from the Greenland Analogue Project (GAP) area near the Russel and Isunnguata Sermia outlet glaciers (Claesson Liljedahl et al. 2016, Harper et al. 2016), from the Jakobshaven Isbrae and adjacent areas (Iken et al. 1993, Lüthi et al. 2002) and Swiss Camp (Ryser et al. 2014). However, we note that the freeze-on Scenario IV (Figure 2-1) appears not to be present along the margins of the contemporaneous Greenland Ice Sheet (MacGregor et al. 2016).

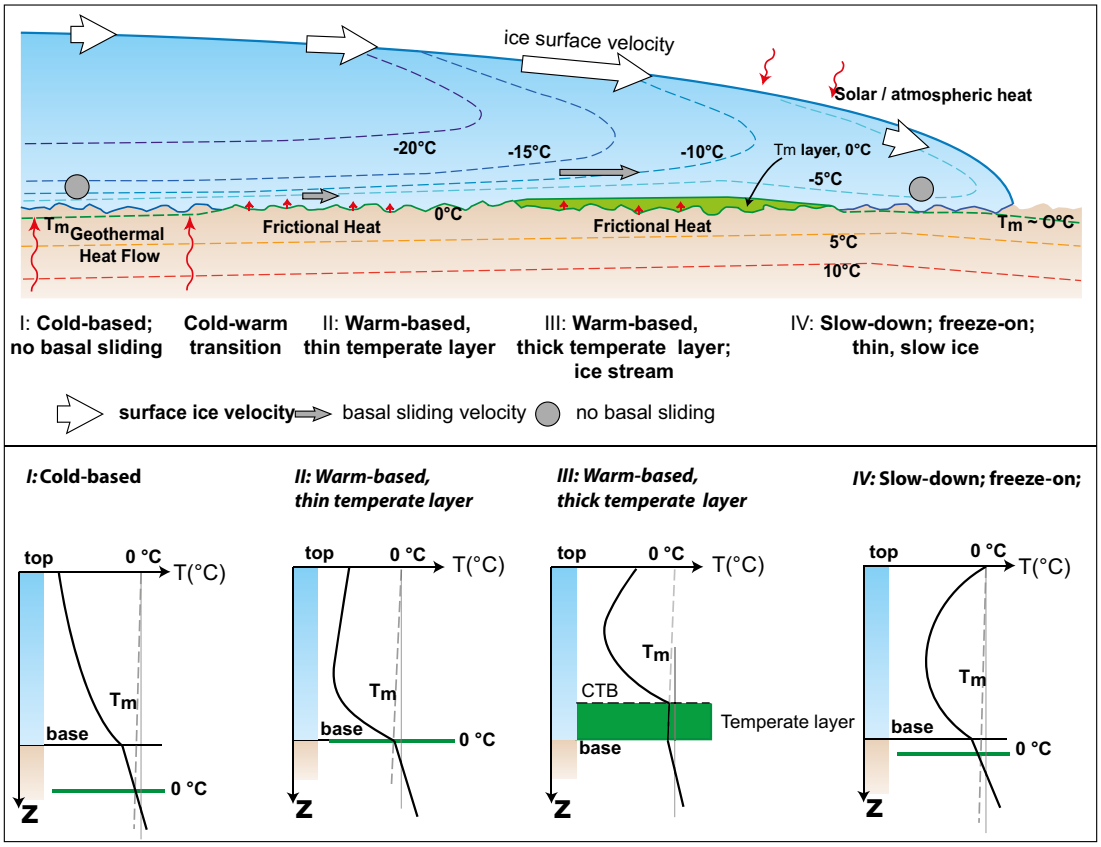

Figure 2-1. *Schematic section from the ice divide to the ice sheet margin, with thermal structure: Temperature gradients for the different parts of the ice sheet are shown in the lower part of the figure. Note that a temperate layer as in case III also may exist without ice stream conditions. T_m = pressure melting temperature, according to the Clausius-Clapeyron relation (dashed line), CTB = cold-temperate boundary. Not to scale. In part modified after Dahl-Jensen (1989).*

2.2 Scenario I: cold-based ice

In the first phase of a glacial cycle, ice-sheet growth is limited to a degree by precipitation, and there is a lag between ice-sheet growth and climatic cooling. Thus, large areas of proglacial permafrost may develop and, during further ice-sheet growth, cold ice can expand over frozen ground or permafrost (Waller et al. 2012). In the area around the ice divide, typically in the centre of the ice sheet, these cold-based conditions may last throughout the glacial cycle (e.g. Kleman et al. 2008, Marshall and Clark 2002, MacGregor et al. 2016). The base of the ice is frozen onto the substrate with a very high static friction coefficient and sliding velocity is practically zero. All ice movement is by internal deformation, with a high viscosity of ice, as the ice temperature is below the melting point. The 0 °C isotherm is well below the bed (Figure 2-1).

2.3 Scenario II: warm-based ice – thin temperate layer

As an ice sheet expands, the thicker ice insulates the base from the cold atmosphere, and geothermal heat warms up the base. In addition, the driving stresses increase and strain heating from internal deformation in the basal part of the ice-sheet also increase the heat budget. At some point, the basal ice temperature rises to the pressure melting point (T_m), and warm-based sliding starts (Figure 2-1). Basal melting commences, and a thin water film or localised channels develop at the ice-bed interface. A thin layer of temperate ice may develop due to frictional heating at the ice-bed interface and strain heating in the basal ice, but this layer is constantly being cooled by colder ice above it (e.g. Dahl-Jensen 1989). In our scenario, the temperate basal layer remains thinner than the height of the obstacles.

At the FOXX and GULL bore holes at Swiss Camp, observed surface ice velocities are c. 70–75 m yr^{-1}, with inferred basal sliding of 50 and 35 m yr^{-1}, respectively (Ryser et al. 2014). In the GAP area, near borehole S5 (GL11-2), the observed surface ice velocity varies between 125–190 m yr^{-1} (Harper et al. 2016), but no sliding speed estimates are available for this site. The basal driving shear stresses (calculated from surface slope and ice thickness) in the GAP project area range from 10–240 kPa, with an average of c. 75–100 kPa (Jezek et al. 2013, Meierbachtol et al. 2016). The thermal conditions in the western part of Greenland Ice Sheet are also discussed by Jaquet et al. (2012) and Harrington et al. (2015), and for the Greenland Ice Sheet as a whole by MacGregor et al. (2016), who suggest that > 43 % of the base of the Greenland Ice Sheet is thawed. Although water is present at the base (likely as a thin film or in distributed channels), meltwater production is limited. However, as this scenario occurs at a distance from the terminus, basal water is unconnected to the terminus, and likely to be confined. In boreholes in upper part of the GAP area, water pressures average at c. 90 % of overburden pressure, with variations between c. 85–98 % (Claesson Liljedahl et al. 2016, Harper et al. 2016).

2.4 Scenario III: warm-based ice – thick temperate layer

Temperate ice has a fundamentally different behaviour than cold ice, with a significantly lower viscosity (e.g. Colbeck and Evans 1973, Duval 1977, Morgan 1991, Krabbendam 2016). We next consider the scenario of warm-based bed, overlain by a thick layer of temperate ice. Thick temperate ice (Figure 2-1) may develop under (at least) two sets of circumstances:

(A) close to the margin, as for example in the present-day GAP area; here temperate ice comprises the entire ice thickness (100–140 m) near the terminus; decreasing to c. 100 m thick in borehole S3 (GL11-1) and S4 (GL12-2) (ice thickness 700 and 820 m respectively) and thinning farther inland (Harrington et al. 2015, Claesson Liljedahl et al. 2016, Harper et al. 2016). It appears that the thick temperate ice layer close to the margin is in part caused by ingress or percolation from surface melt towards the base (e.g. Meierbachtol et al. 2015) and develops under conditions of high surface melt. Surface ice velocities near GL11-1 and GL12-2 vary between c. 90–175 m yr^{-1} (Harper et al. 2016), but no sliding speed estimates are available for these sites. Being near the margin, efficient subglacial channel systems may develop, leading to (temporarily) low water pressures and concomitant high effective pressures (Claesson Liljedahl et al. 2016). Water pressures at the boreholes sites close to the margin varied from 25–98 % of overburden pressure (Harper et al. 2016).

(B) in ice streams. In Borehole D adjacent to the Jakobshavn Isbrae, a temperate layer of ice 30 m thick has been observed below c. 800 m of colder ice (Lüthi et al. 2002); a much thicker temperate ice layer is thought to occur within the trunk of Jakobshavn Isbrae. In such ice-stream conditions, basal melt water production is significant and basal sliding velocities are high (100s m yr^{-1}). Iken et al. (1993) determined high water pressures of 95–100 % of overburden pressure in two boreholes adjacent to the Jakobshavn Isbrae.

2.5 Scenario IV: ice marginal freeze-on

Within a large ice sheet, it is possible that that cold ice overlies warmer ice; this is certainly the case for the Greenland Ice Sheet (Lüthi et al. 2002, Harrington et al. 2015). Near the toe or terminus of the ice sheet, sliding velocities and hence frictional heating decrease, and the cold tongue may reach the base; this may result in freeze-on of the toe of the ice sheet onto its base (Figure 2-1; see also Piotrowski 2006). The substrate a few metres below the bed, however, may still be thawed. This constitutes our 'ice marginal freeze-on' Scenario IV (Figure 2-1). We note that this is not the situation in the present-day GAP project area, but such a situation may develop under different climatic conditions, for instance during a still-stand of the glacial margin retreat, or possibly because the Pleistocene Fennoscandian Ice Sheet was colder internally than the present-day Greenland Ice Sheet. Because freeze-on likely occurs close to the margin of the ice sheet, with a steep ice-slope, there is potential for a considerable water pressure gradient. As the bed is (locally) frozen and drainage is impeded, but water production up-ice may continue (e.g. surface melt water that finds its way to the base), high water pressures may build up below the frozen-thawed boundary within the substrate (e.g. Waller et al. 2012, Lönnqvist and Hökmark 2013). These water pressures may approach or, under certain circumstances, exceed overburden pressure. This scenario requires cold ice to be present above the base, and a relatively thin temperate ice layer as this layer needs to freeze during slow-down near the terminus. This scenario does not appear to occur in the contemporaneous Greenland Ice Sheet (MacGregor et al. 2016); but cannot be excluded for the Fennoscandian Ice sheet in times of slow down or still stand during glacial retreat.

Table 2-1. Parameter used for different scenarios. For constants used, see Appendix 1.

	Scenario I: Cold-based	**Scenario II: Warm-based – thin temperate ice**	**Scenario III: Warm-based – thick temperate ice**	**Scenario IV: Ice marginal freeze-on**
Ice thickness h_i (m)	100, 1 000	100, 1 000	100, 1 000	100
Water pressure (% of overburden pressure)	0	90, 95, 98	50, 90, 98	0, 90, 100
Friction coefficient, μ	0.6, 0.9	0.3, 0.6	0.3, 0.6	0.3, 0.6
Sliding velocity (m yr^{-1})	0	5, 10, 25	50, 100, 200	0
Basal shear stress (kPa)	20, 100, 150		100, 200, 500 (*)	20, 50, 100
Ice viscosity η (Pa s)	n/a	1.3×10^{12} , 1.3×10^{13}	1.3×10^{11}	n/a

(*) In case of fast basal melting only (see Cohen et al. 2005).

3 Forces, stresses and pressures under consideration

Initially, we consider a block of bedrock as a cube with equal sizes, so that $V = L^3$ (Figure 3-1). The block rests on a horizontal surface, separated from the underlying bedrock by a fracture (joint), but this joint may be rough or cemented. Most tors do have such a joint at or near its base, because the surrounding bedrock has typically been eroded down to the level of a particular sub-horizontal joint surface. Sub-horizontal fractures also occur in the Forsmark area, and upstanding rock blocks here locally have sub-horizontal fractures at or near their base (Lagerbäck et al. 2005, Forssberg et al. 2007; and observations by the authors of this report). In reality, an upstanding block or tor may have multiple joints and comprise multiple blocks: in that case the modelling is applicable to an individual block making up the larger mass, unless a block is buttressed by another block occurring down-ice.

We consider that water may penetrate the joint and has a certain water pressure P_w. We further assume that there is no ice below the block, or at least no ice at cryostatic pressure. The weight of the block and the ice above it creates a vertical normal force F_z on the basal joint, which creates a resisting force F_{rx}, depending on the friction coefficient along the basal joint. The block is covered by ice with thickness h_i, resulting in a cryostatic pressure P_i. Due to ice flow, there is an overall shear stress at the base of the ice sheet. The ice also exerts a direct push force F_{dx} against the block, which comprises a number of components, as detailed below.

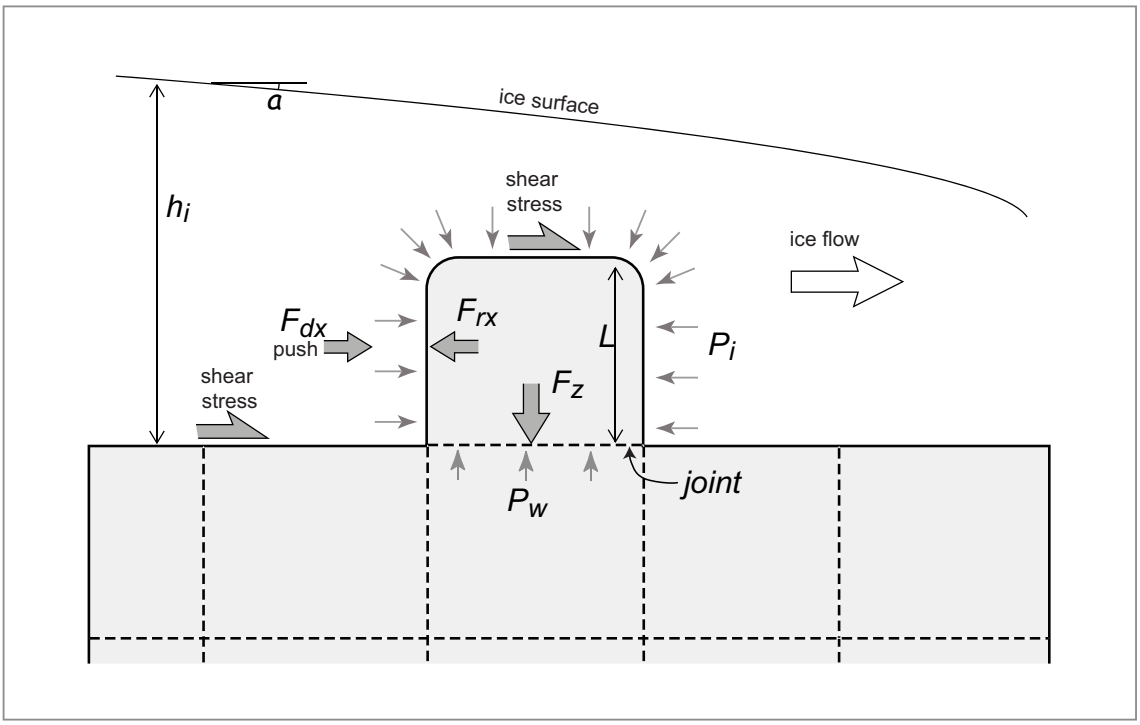

Figure 3-1. *Schematic drawing showing different forces, stresses and pressures on a block at the bed of an ice sheet – not to scale. F_{dx} = driving force; F_{rx} = resisting force; F_z = normal force on basal joint; h_i = ice thickness; L = size of block; P_i = cryostatic pressure; P_w = water pressure.*

4 Resisting forces

The resisting force of a block sticking out of the surrounding bed is in essence given by:

$$F_{rx} = F_z \mu_{rr} \quad (4\text{-}1)$$

where F_{rx} is the horizontal resisting force, μ_{rr} the rock-rock friction coefficient along the basal joint at the base of the block, and F_z the normal force acting vertically on the basal joint. The normal force F_z has several components, all depending on the size of the block and the local glaciological conditions, such as temperature, ice thickness and water pressure. The normal force includes the following components:

$$F_z = F_{bz} + F_{iz} + F_{mz} \quad (4\text{-}2)$$

where F_{bz} is the buoyant weight of the block; F_{iz} any force (weight) exerted by the overlying ice and F_{mz} the drag force exerted by ice flowing vertically downward due to basal melting.

The treatment of the normal force acting on a block is related to the clast-bed contact forces as explored by Cohen et al. (2005), Byers et al. (2012) and Krabbendam et al. (2017), but differs in that it is assumed here that beneath the block there is no ice under cryostatic pressure present. Also, the much larger size of a block compared to a clast means that some of the formulation needs to be different.

4.1 Buoyant weight

The buoyant weight of the block is given by:

$$F_{bz} = L^3 (\rho_r - \rho_w) g \text{ (in N)} \quad (4\text{-}3)$$

where L is the length of the side of the cube (so that L^3 equals the volume), ρ_r is the density of rock, ρ_w is the density of water, and g is the standard acceleration of gravity (see Appendix 1 for a list of constants and variables used). The above is valid if the block is immersed in water, i.e. in a temperate ice with a 'water table' in the ice that is higher than the block, and if there is a fracture/joint plane beneath the block that is water filled and at equal water pressure as the surrounding ice/rock interface.

Note that in a cold-based environment, no water is present so that the weight is increased to:

$$F_{bz} = L^3 \rho_r g \text{ (in N)} \quad (4\text{-}4)$$

4.2 The effective weight of the overlying ice

The weight of the overlying ice (in essence the effective pressure multiplied by area) also plays a significant role, and is given by:

$$F_{iz} = (P_i - P_w) A = (P_i - P_w) L^2 \quad (4\text{-}5)$$

where P_i is the cryostatic pressure, P_w the water pressure and A the surface area of the top of the block, which is L^2 for a cubic block. This equation has been proposed by Boulton (1979) to calculate the force of a clast on the glacier bed, but discarded by other researchers, on the basis that clasts are largely surrounded by ice under cryostatic pressure (e.g. Hallet 1979, Cohen et al. 2005). However, the weight of the ice needs to be taken into account for a tor or cnoc resting with a tight joint onto the bed below, because is not likely to have ice beneath it that transfers the cryostatic pressure of the surrounding ice.

Under very high water pressures, where $P_w > P_i$, the force becomes negative, and may want to 'lift off' the block. Whilst this situation is not stable for long duration and over large areas, P_w of up to 105 % has been measured close to the Greenland Ice Sheet terminus for short periods of time (< 1 day; Claesson Liljedahl et al. 2016). The situation is also relevant for the hydraulic jacking along

sub-horizontal fractures deeper in bedrock that appears to have occurred on the Fennoscandian shield (Talbot 1999, Pusch et al. 1990, Forssberg et al. 2007); although the depth at which hydraulic jacking may occur is disputed (Lönnqvist and Hökmark 2013, Talbot 2014).

In formulation it is easier to rewrite Equation (4-5) with the variables of ice thickness and relative effective pressure P_{ref}:

$$F_{iz} = h_i\, g\, \rho_i\, L^2\, P_{ref} \quad (4\text{-}6)$$

where h_i is the ice thickness, ρ_i the density of ice and the relative effective pressure given by:

$$P_{ref} = \frac{P_i - Pw}{P_i} \quad (4\text{-}7)$$

so that if $P_w = 0$ then $P_{ref} = 1$ and if $P_w = P_i$ then $P_{ref} = 0$. In cold ice, water pressure can be seen as 0, and hence $P_{ref} = 1$. In the discussion and the diagrams, however, water pressure is expressed as a percentage of the cryostatic pressure (e.g. $P_w = 90$ %).

Because F_{iz} rises with the power of 2 of the size of the block (Equation 4-6), whereas F_{bz} rises with the power of 3 (Equation 4-4), F_{bz} becomes more important for larger blocks.

4.3 Drag force by basal melting

A further contribution to the normal force is potentially made by viscous drag exerted by ice moving vertically downwards to the bed, due to basal melting. This may occur if basal melting rates are high, for instance during periods of fast ice flow, or in areas of elevated geothermal heat flow. As ice moves vertically towards the bed, it flows in a viscous manner around the block. This viscous flow creates a drag force; for *small* clasts (< 50 cm) this is seen as the largest and most important force with which a clast is pressed upon the bed (Cohen et al. 2005, Byers et al. 2012, Krabbendam et al. 2017).

Melt production, expressed as a vertical velocity towards the bed U_{mz}, is determined by the geothermal heat production and the frictional heat production on the bed (e.g. Brinkerhoff et al. 2011). Frictional heat production in turn is determined by the effective pressure, the sliding velocity and the friction coefficient of the ice sliding over the bed, so that the vertical velocity due to melting can be expressed as (e.g. Krabbendam 2016):

$$U_{mz} = \frac{Q_{geo} + \mu_{ir}\ (P_i - P_w)\ U_{sl}}{H_{ice}\ \rho_{ice}} \quad (4\text{-}8)$$

where Q_{geo} is the geothermal heat production (typical values ~ 30–85 mW m^{-2} for Fennoscandia; e.g. Näslund et al. 2005); μ_{ir} is the ice-rock friction coefficient; U_{sl} is the ice sliding velocity along the bed and H_{ice} is the heat of fusion of ice (334 kJ kg^{-1}).

The force F_{mz} exerted by viscous drag of a viscous material moving a spherical obstacle may be described by Stoke's Law:

$$F_{mz} = 6\,\pi\, r\, \eta\, U_{mz}\ (\text{sphere}) \approx\ 10\, L\, \eta\, U_{mz}\ (cube) \quad (4\text{-}9)$$

where r is the radius of the sphere; η = the viscosity of the material and U_{mz} the velocity, in this case taken as vertically downward (e.g. Furbish 1997, see also Byers et al. 2012). For a cube, $6\pi r$ can be reasonably approximated as 10 L. At the melting temperature (i.e. in so-called temperate ice), $\eta \sim 1.3 \times 10^{11}$ Pa s (e.g. Byers et al. 2012). Basal melt rates in Greenland have been modelled to lie between 0–25 mm yr^{-1} (e.g. Aschwanden et al. 2012) although below the North East Greenland Ice Stream (NEGIS), basal melt rates in the order of 80–150 mm yr^{-1} have been deduced from long-term basal melting of isochrones (Fahnestock et al. 2001).

Stoke's Law relates the force of a viscous material flowing around a sphere under laminar flow with low Reynolds numbers (Re << 1). The low Reynolds number is clearly satisfied (Re ~ $10^{-12\ \text{to}\ -13}$ for ice with an obstacle length of 1–10 m, see Appendix 2). Stoke's Law has been tested for the case of laminar flow of very small particles in a fluid of medium viscosity, for instance the settling of silt and

clay particles in water. Whether Stoke's Law is applicable to large, metre-scale obstacles in a very viscous material such as ice is uncertain (see discussion in Section 7.3). Another possibility may be to use a general drag equation, but that has not been performed for this study.

4.4 Normal forces for different scenarios

In **cold-based ice (Scenario I)**, basal melting is zero and water pressure can be ignored, so that the normal force is the weight of the block F_{bz} plus the full weight of the overlying ice F_{iz}. In that case:

$$F_z = F_{bz} + F_{iz} = L^3 \rho_r g + h_i g \rho_i L^2 \text{ (in N)} \quad (4\text{-}10)$$

For blocks between 5 and 15 m in length under 100 m of ice, the typical range of the total vertical force F_z is 25–300 MN (Figure 4-1 A); with an ice thickness of 1 000 m this increases to 200 to > 1 000 MN (Figure 4-2 A).

In the **warm-based** ice scenarios **(Scenarios II and III)** it can be assumed that the block is immersed in water. This lowers the buoyant weight of the block, and lowers the effective load of the overlying ice, depending on the water pressure at the base.

In that case:

$$F_z = F_{bz} + F_{iz} = L^3 (\rho_r - \rho_w) g + h_i g \rho_i L^2 P_{ref} \quad (4\text{-}11)$$

In the **warm-based ice – thin temperate ice (Scenario II)**, water pressures are likely to be high (see Section 2.3 and Claesson Liljedahl et al. 2016), and we vary water pressures between 90–98 %. For blocks between 5 and 15 m under 100 m of ice, the typical range of the total vertical force F_z is 10–70 MN (Figure 4-1 B); under 1 000 m of ice this increases to 50–250 MN (Figure 4-2 B), showing a strong dependence on ice thickness. Overall, the normal force under the warm-based scenario is significantly lower than in the cold-base scenario.

In an **warm-based ice – thick temperate ice (Scenario III)** with high ice sliding velocities as in an ice stream, significant basal melting may occur due to increased frictional heating, in which case a viscous drag force F_{mz} maybe exerted onto the block. The total normal force then becomes:

$$F_z = F_{bz} + F_{iz} + F_{mz} = L^3 (\rho_r - \rho_w) g + h_i g \rho_i L^2 P_{ef} + 10 L \eta U_{mz} \quad (4\text{-}12)$$

As is seen from Figure 4-1 B and 4-2 C, the contribution from basal melting to the vertical force is minimal, and is ignored hereafter (at very small block sizes, < 20 cm, the drag force is important, and is the dominant force for clasts < 4 cm; e.g. Byers et al. 2012).

In this scenario, water pressures are likely highly variable: e.g. close to the margin in the GAP area, water pressure below 50 % have been observed (see Section 2.3; Claesson Liljedahl et al. 2016), whereas in ice stream scenarios away from the terminus, water pressures may remain high and approach overburden pressure (e.g. Iken et al. 1993); we vary water pressures between 50–98 %.

For blocks between 5 and 15 m in length under 100 m of ice, the typical range of the total vertical force F_z is 5–100 MN, with the highest resisting forces under the lowest water pressures (Figure 4-1 C). With an ice thickness of 1 000 m this increases to 100–1 000 MN (Figure 4-2 C). Overall, the normal forces in this scenario are lower than under cold ice, except at low water pressures. There is a strong dependency on water pressure, ice thickness and block size.

In the marginal **freeze-on scenario IV**, the top of the block is frozen, so that the full weight of the ice is pressing upon the top of the block. Basal melting will be zero and the water pressure between the top of the block and the ice is taken as effect zero. However, if the pressure melting point is just below the ice-bed, it is possible that water may occur below the block. In that case, the weight of the block can be taken as the buoyant, 'immersed' weight (Equation (4-3)). Moreover, such water maybe under highly variable pressures; if a sufficiently high pressure gradient occurs in the up-ice region, water pressures may reach overburden pressure (P_w = 100 %; P_{ref} = 0). The normal force of the block is formulated as follows:

$$F_z = F_{bz} + F_{iz} = L^3 (\rho_r - \rho_w) g + h_i g \rho_i L^2 P_{ref} \quad (4\text{-}13)$$

The freeze-on scenario is unlikely for thick ice, so these results are only shown for an ice thickness of 100 m (Figure 4-1 D). For blocks between 5 and 15 m under 100 m of ice the typical range of the total vertical force F_z is 30–250 MN, similar but slightly lower than in the cold-based scenario. However, if high water pressures develop, the vertical normal forces drop dramatically to 5–70 MN at a water pressure of 90 %, whereas at a water pressure of 100 % (e.g. $P_{ref} = 0$), the only remaining force is the immersed buoyant weight, amounting to a mere 5–50 MN (blue/black dashed line, Figure 4-2 D).

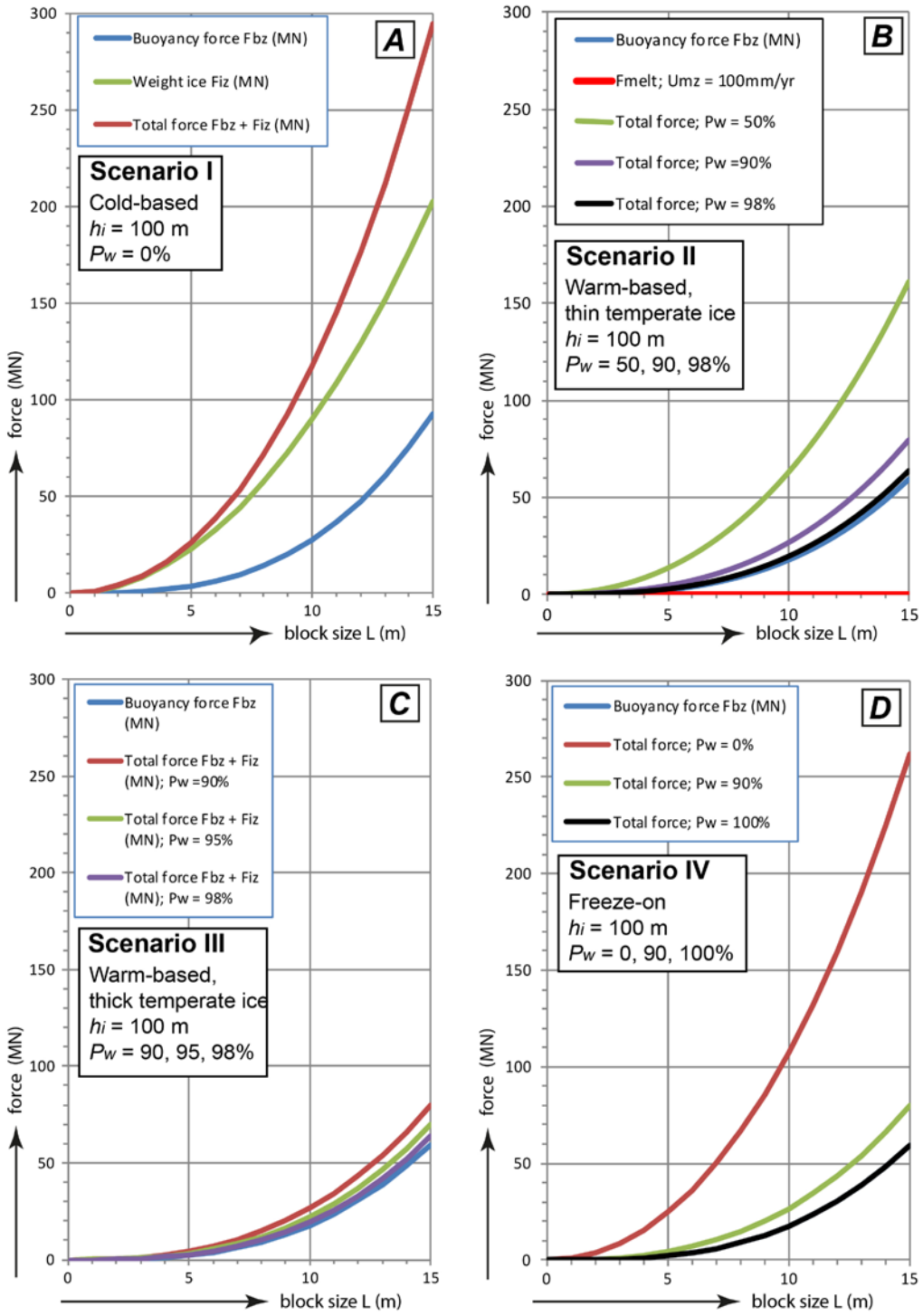

Figure 4-1. *Normal force (in MN) exerted by a block on its base, as a function of block size (in m) for different glaciological scenarios. Ice thickness = 100 m; showing individual F_{bz} and F_{mz} and total force $F_z = F_{bz} + F_{iz} + F_m$, variable water pressure indicated. (A) Scenario I, Cold-based. (B) Scenario II: Warm-based; thin temperate ice, with drag by basal melting ignored. (C) Scenario III: Warm-based; thick temperate ice, with drag by basal melting. (D) Scenario IV, freeze-on, with buoyant weight (water below block), but no basal melting and full weight of ice above.*

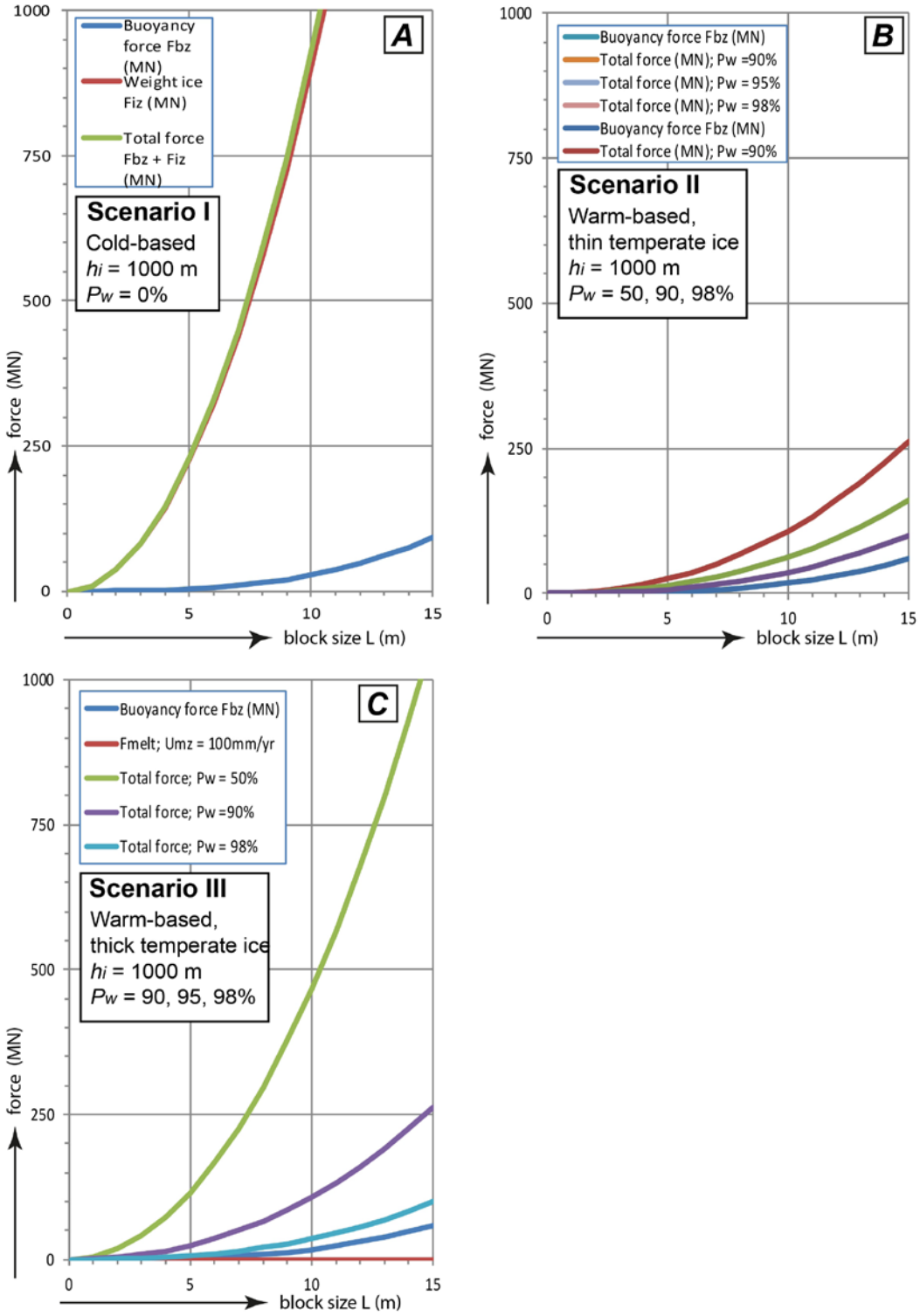

Figure 4-2. *Normal force (in MN) exerted by block on its base, as a function of block size (in m). As Figure 4-1, but with ice thickness of 1 000 m; showing individual F_{bz} and F_{mz} and total force $F_z = F_{bz}+F_{iz}+F_m$. Variable water pressure indicated. (A) Scenario I, Cold-based. (B) Scenario II: Warm-based; thin temperate ice, with drag by basal melting ignored. (C) Scenario III: Warm-based; thick temperate ice, with drag by basal melting.*

4.5 Friction coefficient and resisting forces

We assume here that the contact between the block and the bed is a joint. The friction along that joint has a rock-on-rock friction, which can vary widely: Ramana and Gogte (1989) report rock-rock friction coefficients between μ_{rr} = 0.5–0.8, with crystalline rocks at the higher end and mica-bearing rocks at the lower end of this spectrum. However, the joint contact maybe rough and have asperities, and may also be partially cemented, increasing the overall friction coefficient. Conversely, a layer of granular material (sand, silt, clay) may be present (for instance due to weathering or subglacial meltwater deposition), which may lower the friction coefficient.

In the case of a frozen substrate, any water film present will freeze within the joint. The friction coefficient of parts of the joint will then have static ice-rock friction coefficient, which will be at the high end, and possibly even exceed 1. The very steep (> 45°) ice faces in Alpine regions suggest that it is possible that the static ice-rock friction coefficient exceeds 1. Overall, we show here results with friction coefficients of μ_{rr} = 0.3, 0.6 and 0.9.

As described above, the overall resisting force is the given by:

$$F_{rx} = F_z \mu_{rr} \tag{4-14}$$

For the **cold-based Scenario I**, where high friction coefficients (μ_{rr} = 0.6–0.9) are justified and the normal forces are high, the resultant resisting forces are high (Figure 4-3): about 100 MN for an ice thickness of 100 m for a 10 m block, but increasing to 600–800 MN for an ice thickness of 1 000 m (Figure 4-3 A). The resisting force increase both with friction coefficient, ice thickness and block size.

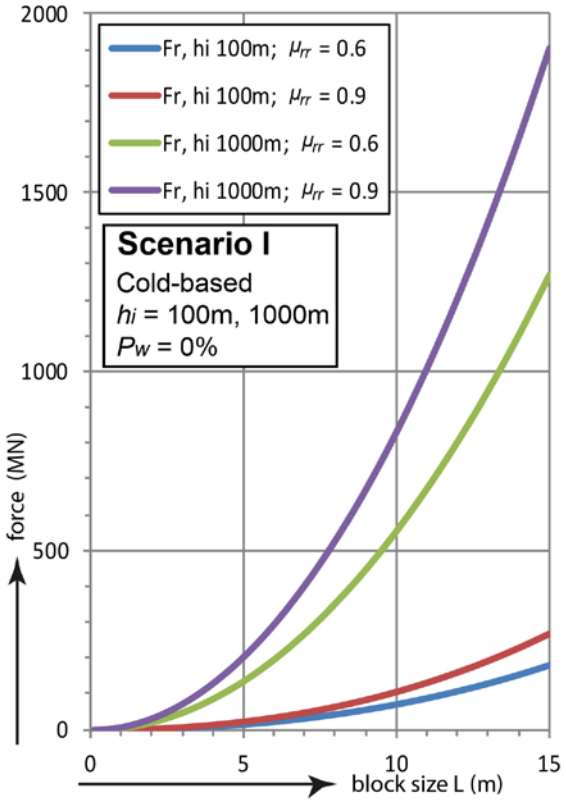

Figure 4-3. *Horizontal resisting forces (Fr, in MN) as calculated from normal forces on the base of a block, with different friction coefficients, as a function of block size (in m). Cold based scenario, with high friction coefficients (μ_{rr} = 0.6–0.9); ice thickness = 100 m and 1 000 m.*

For the **warm-based ice – thin temperate ice (Scenario II)** we take low friction coefficients (μ_{rr} = 0.3–0.6) as the base of the block is not frozen. The resisting forces in this scenario are significantly lower than in the cold-based scenario (Figure 4-4 A, B). The high water pressure, combined with the lower friction coefficient result in resisting forces below 20 MN for a 10 m block under 100 m of ice (Figure 4-4 A), and below 60 MN beneath 1 000 m of ice (Figure 4-4 B). The lowest resisting forces occur at the highest water pressures (98 %) and the lowest friction coefficients.

The **warm-based ice – thick temperate ice (Scenario III)** results are similar to those of Scenario II (Figure 4-4), but are highly dependent on the water pressures, which we vary between 50–98 % of overburden pressure. The results (Figure 4-4 C) show that resisting forces range from < 5–40 MN for a 10 m block under 100 m ice, depending on friction coefficient and water pressure. Under 1 000 m of ice the resisting forces are substantially higher, and range from c. 10–300 MN for a 10 m block, with the lowest resisting forces with the highest water pressure and the lowest friction coefficients.

The **freeze-on Scenario IV** is hybrid in the sense that there is water at the base of the block, so lower friction coefficients (μ_{rr} = 0.3–0.6) are justified, but there is no water above the block, so that the full weight of the ice contributes to the normal force. As a consequence the resisting forces are high (Figure 4-5): c. 30 MN for a 10 m block under 100 m ice with a low friction coefficient, to c. 60 MN for a 10 m block with a higher friction coefficient. However, if high water pressures occur (90 % and 100 % are shown), the resisting forces drop dramatically to less than 20 MN for a 10 m block. Only results for an ice thickness of 100 m are shown.

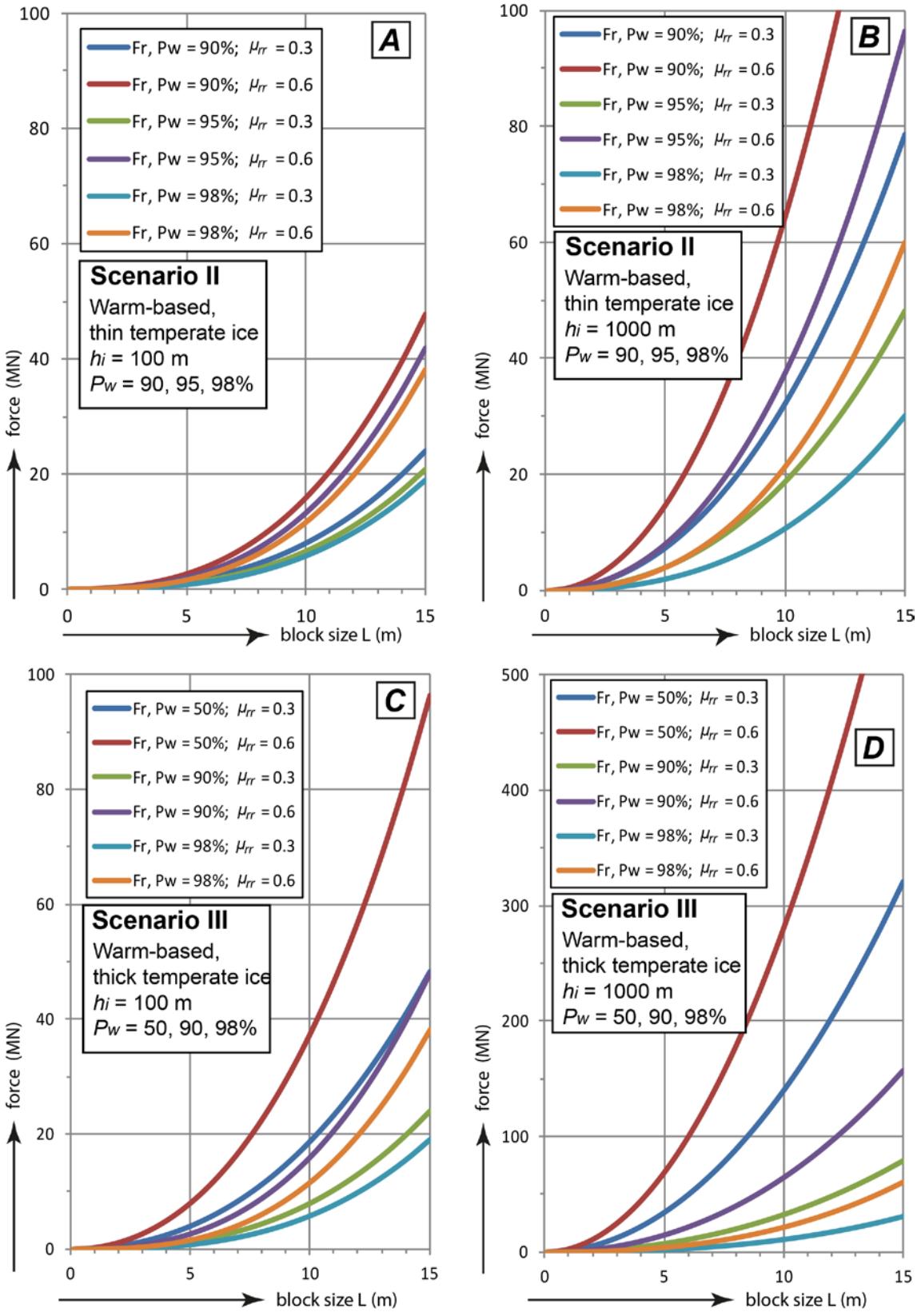

Figure 4-4. *Horizontal resisting forces (F_r, in MN) as calculated from normal forces on the base of a block, with different friction coefficients, as a function block size (in m). (A) Warm-based thin temperate ice Scenario II, with low friction coefficients (μ_{rr} = 0.3–0.6), and variable water pressures (90, 95, 98 %); ice thickness = 100 m. (B) as A, ice thickness = 1 000 m (C) Warm-based, thick temperate ice Scenario II, with low friction coefficients (μ_{rr} = 0.3–0.6), and variable water pressures (50, 90, 98 %); ice thickness = 100 m. (D) as A, ice thickness = 1 000 m.*

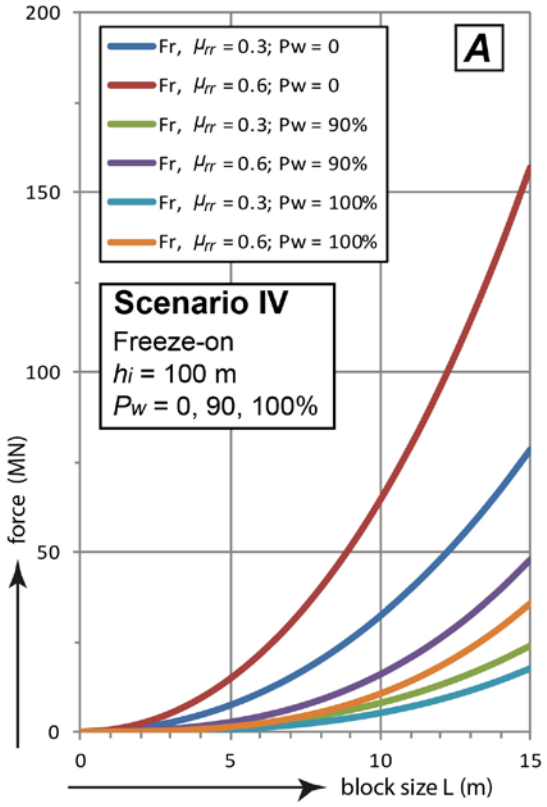

Figure 4-5. *Horizontal resisting forces (Fr, in MN) as calculated from normal forces on the base of a block, with different friction coefficients, as a function block size (in m). Freeze-on scenario, with low friction coefficients (μ_{rr} = 0.3–0.6); ice thickness = 100 m, and varying water pressure (0, 90, 100 %).*

5 Driving forces and block removal

5.1 Driving forces

The driving force acting onto a block is provided by ice flow pushing against, and shearing around and over the block. Two approaches can be taken to quantify this force. We can either assume that the main driving force is provided by viscous drag exerted by ice with a particular velocity and viscosity, deforming around the block, or alternatively, we can use the overall driving shear stress at the base of the ice sheet, and assume that this basal shear stress works wholly on the vertical stoss face. The first case may be described by Stoke's Law, adapted for a cube:

$$F_{ix} = 6\,\pi\,r\,\eta\,U_{sl}\ (\text{sphere}) \approx 10\,L\,\eta\,U_{sl}(cube) \qquad (5\text{-}1)$$

where U_{sl} is the ice sliding velocity towards the block, and η the viscosity for ice, which varies strongly with ice temperature and stress. The problem with this approach is that the pushing force only increases linearly with the block size, which is rather counterintuitive as one would expect this to increase linearly with the exposed surface area. Whether Stoke's Law is applicable for ice with such metre-size obstacles is discussed in Section 7.3.

Using the second approach, if a rock obstacle such as a tor is isolated and sufficiently large, the normal stress acting horizontally onto the stoss face of the obstacle is approximately equal to the basal driving shear stress. The overall shear stress at the base of glacier can be simplified to:

$$\tau_{dx} = \rho_i g h_i \sin\alpha \qquad (5\text{-}2)$$

where α is the slope of the ice. The advantage of this method is that basal shear stresses are fairly well constrained beneath modern ice sheets, with typical values between 20–150 kPa (e.g. Paterson 1994). For the GAP area, Jezek et al. (2013) calculated basal shear stresses ranging from c. 20–220 kPa, with the highest stresses occurring in overdeepenings. MacGregor et al. (2016) calculate basal shear stresses from < 10 to > 160 kPa across the entire Greenland Ice Sheet, with the lowest shear stresses (< 70 kPa) coinciding with the cold-based interior of the ice sheet, and the highest near the warm-based margins.

In addition, ice moving along the top and lateral surfaces of the block also exerts a shear stress onto the block. In warm-based conditions, there is a very low friction coefficient between ice and rock, with a water film in between: measured friction coefficients in subglacial environment suggest μ_{ir} = ~ 0.01–0.2 (Budd et al. 1979, Iverson et al. 2003, Cohen et al. 2005, Zoet et al. 2013). If the system behaves according to a simple Coulomb friction model, friction is in essence determined by the debris concentration, and will be low.

However, under conditions of high basal melt rates, in subglacial experiments beneath the Svartisen Glacier, Cohen et al. (2005) measured very high basal shear stresses (80–500 kPa) despite low overall friction coefficients (μ_{ir} = ~ 0.05–0.08); and it appears a simple Coulomb friction model is not applicable. Cohen et al. (2015) suggested this was caused by very high contact forces between debris particles and the bed, which are caused by viscous drag around the debris particle, which in turn are caused by high basal melting rates. Thus, in Scenario III, where high basal melt rates are possible we also model the driving forces using high basal shear stresses.

In a cold-based environment, the ice is frozen onto the block. In that case, the *dynamic* ice-rock friction coefficient can approach that of rock-rock friction, with μ_{ir} = 0.3–0.7 (Zoet et al. 2013). The static friction coefficient, however, may be as high as 1 so that the shear stress of a lateral or top side maybe equal to the normal stress on the stoss side.

In Figures 5-1 to 6-3, the resisting forces are plotted as solid lines, and the driving forces as dashed lines.

5.2 Cold-based ice – Scenario I: Driving forces and block removal

In the cold-based scenario, the approach whereby the driving force is derived from a static shear stress is most appropriate, since viscous ice flow is low. In this scenario there is not only is a direct push onto the stoss-side, but also a shear stress acting on the top and the sides of the block, because the ice is frozen onto the block. This shear stress is broadly equal to the overall shear stress (see Section 5.1). For a cubic block, with one stoss side, a top side and two lateral sides, this means the driving force can be approximated as:

$$F_{dx} = 4\,L^2\tau_{dx} \tag{5-3}$$

Under most conditions, the resisting forces exceed the driving forces, and no block removal would occur (Figure 5-1). The only conditions under which driving forces approach the resisting forces occur if the overall driving stress is very high (150 kPa), the ice is thin (100 m) and the friction coefficient at the base is low (μ_{rr} = 0.6), that is as low as can be expected in a frozen base (red lines on Figure 5-1 B, which is an enlarged version of Figure 5-1 A). Although the two curves cross each other, they do so at a low angle. This means that the difference between the driving and resisting forces is not strongly dependent on block size. This implies in turn that cold ice will either not move any block, or it will sweep all or most blocks (except possibly the largest ones), but only under the favourable conditions described. We note that in the Greenland Ice Sheet, those areas that are likely to be cold-based have shear stresses less than 70 kPa (MacGregor et al. 2016). This suggests that the scenario of very high shear stresses (> 100 kPa) are not realistic and that in general blocks will not move. This is consistent with the survival of tor bedforms in some glaciated areas thought to have been largely cold-based throughout glaciation (e.g. Hättestrand and Stroeven 2002, Hall and Glasser 2003).

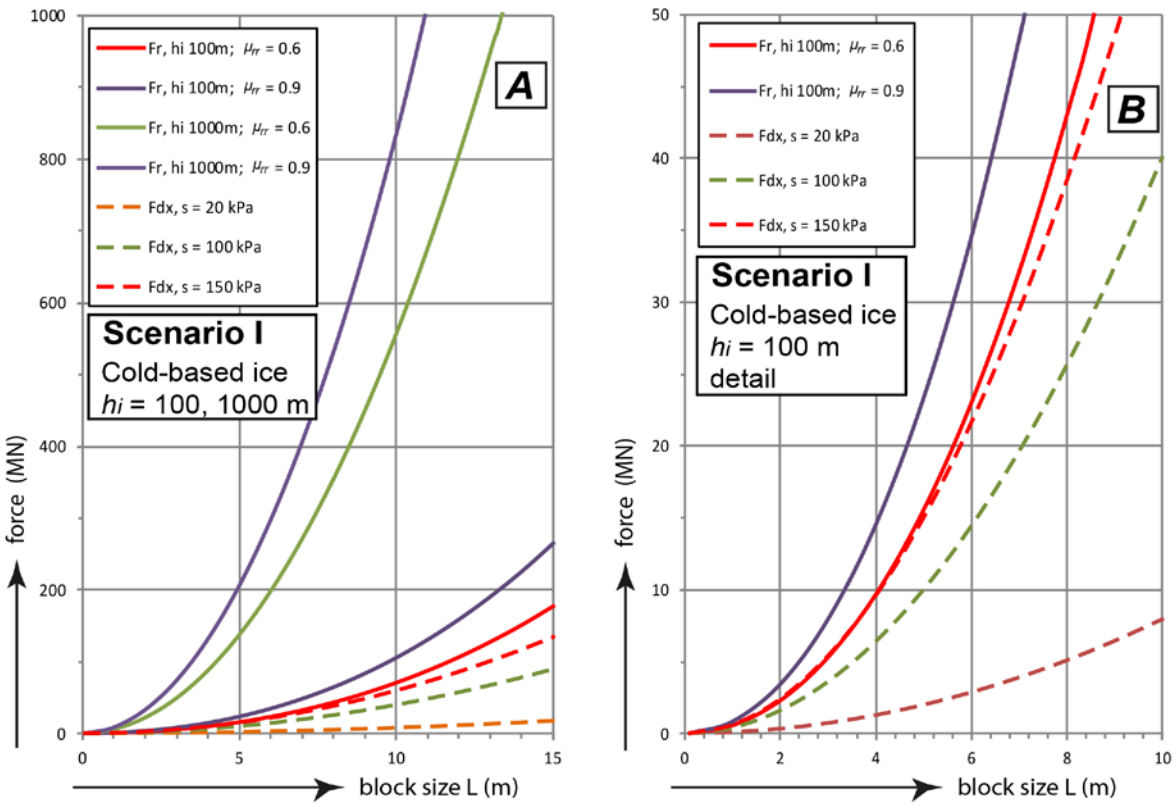

Figure 5-1. *(A) Driving forces (dashed lines) and resisting forces (solid lines) (in MN) as a function of block size (in m) for Cold-based Scenario I. (B). Same dataset, showing detail for blocks < 10 m under 100 m ice only. s = basal shear stress.*

5.3 Warm-based ice – thin temperate layer Scenario II: Driving forces and block removal

In the warm-based – thin temperate ice, Scenario II, the bed below the block is thawed (Figure 2-1) and relatively low rock-rock friction coefficients along the basal joint are justified (μ_{rr} = 0.3–0.6). We look both at the cases where the driving force is generated by the applied shear stress and by viscous drag. In the case of applied shear stress, we note that on the top and lateral sides, the ice-bed contact is now thawed. The dynamic friction along these contacts is very low (μ_{ir} ~ 0.01–0.2; Budd et al. 1979, Iverson et al. 2003, Zoet et al. 2013), and only contributes a minute amount to the overall driving force: it is ignored here. Thus we let the driving shear stress act only on the stoss side, so that:

$$F_{dx} = L^2 \tau_{dx} \quad (5\text{-}4)$$

When using the shear stress approach, the driving forces exceed the resisting forces in the case of high water pressures, and high shear stresses (Figure 5-2 A, B). Under thin ice (100 m; Figure 5-2 A), block removal may occur for instance with a shear stress of 100 kPa, and high water pressures (Pw = 98 %), in case of both low and medium friction coefficients. However, under thick ice (1 000 m), driving forces remain below resisting forces in all but the most favourable conditions (green line in Figure 5-2 B). Where the curves for driving and resisting force curves are close, they are broadly parallel, which suggests that the effect of block size is not significant. In practice this means that the glaciological conditions (ice thickness and driving stress) are more important than block size: either the 5–15 m long blocks stay in place, or they move, regardless of size.

If the driving force is calculated from the viscous drag, using Stoke's Law (Equation 4-9), the problem arises as to what value for the ice viscosity parameter should be used. In the warm-based, thin temperate ice scenario, the base is thawed, but the ice above the bed is 'cold', i.e. below the pressure melting point. Temperate ice may have a constant viscosity (i.e. it may behave as a near-Newtonian viscous material; Chandler et al. 2008, Byers et al. 2012; see Krabbendam 2016 and Section 7.3. herein); Byers et al. (2012) determined a viscosity of $\eta = 1.3 \times 10^{11}$ Pa s for temperate ice. In contrast, cold ice obeys a power-law creep, so that the effective viscosity is a function of the deviatoric stress via a stress exponent (i.e. cold ice is non-Newtonian), as well as being strongly dependent on the temperature (e.g. Glen 1955, Alley 1992, Paterson 1994). Thus, there is no single value for the viscosity that can be used for Stoke's Law. Perhaps rather arbitrarily, we use a viscosity ten times higher ($\eta = 1.3 \times 10^{12}$ Pa s) than that of temperate ice; ice experiments under c. 100 kPa deviatoric stress appear to suggest this is reasonable (Morgan 1991; see also Krabbendam 2016). We also show one example (with a sliding velocity of 10 m yr^{-1}) of an even higher viscosity ('cold-high viscosity'; $\eta = 1.3 \times 10^{13}$ Pa s). We also limit the basal sliding velocity to 25 m yr^{-1}, since at higher velocities it is likely a thicker temperate layer of ice develops, which is described in Scenario III (Section 5.4).

The results (Figure 5-2 C, D) show that driving forces by viscous drag exceed resistance in the case of high sliding velocities and high viscosity. Because the driving forces increase linearly with block size, whereas the resisting forces increase exponentially, there is a strong sorting effect: blocks < 5 m are removed in almost all cases, whereas blocks > 10 m are only removed under high sliding velocities. Under thin ice (100 m) almost all blocks are removed, whereas under thick ice blocks > 5–7 m remain except under very high viscosities or sliding velocities (brown and black dashed lines in Figure 5-2 D). The likelihood of block removal is also strongly dependent on the chosen viscosity: for a sliding velocity of 10 m yr^{-1}, many large blocks (> 7 m) stay in place with a low viscosity (yellow dashed line on Figure 5-2 D), whereas with a highest viscosity all blocks are removed (black dashed line on Figure 5-2 D).

The results of the two methods (basal shear stress and viscous drag) do not agree: with viscous drag almost all blocks < 10 m are removed under most conditions (for thin ice, Figure 5-2 B), whereas with basal shear stress, most block will remain. This represents a major uncertainty, likely related to the use of Stoke's law for viscous drag around large obstacles (Section 7.3).

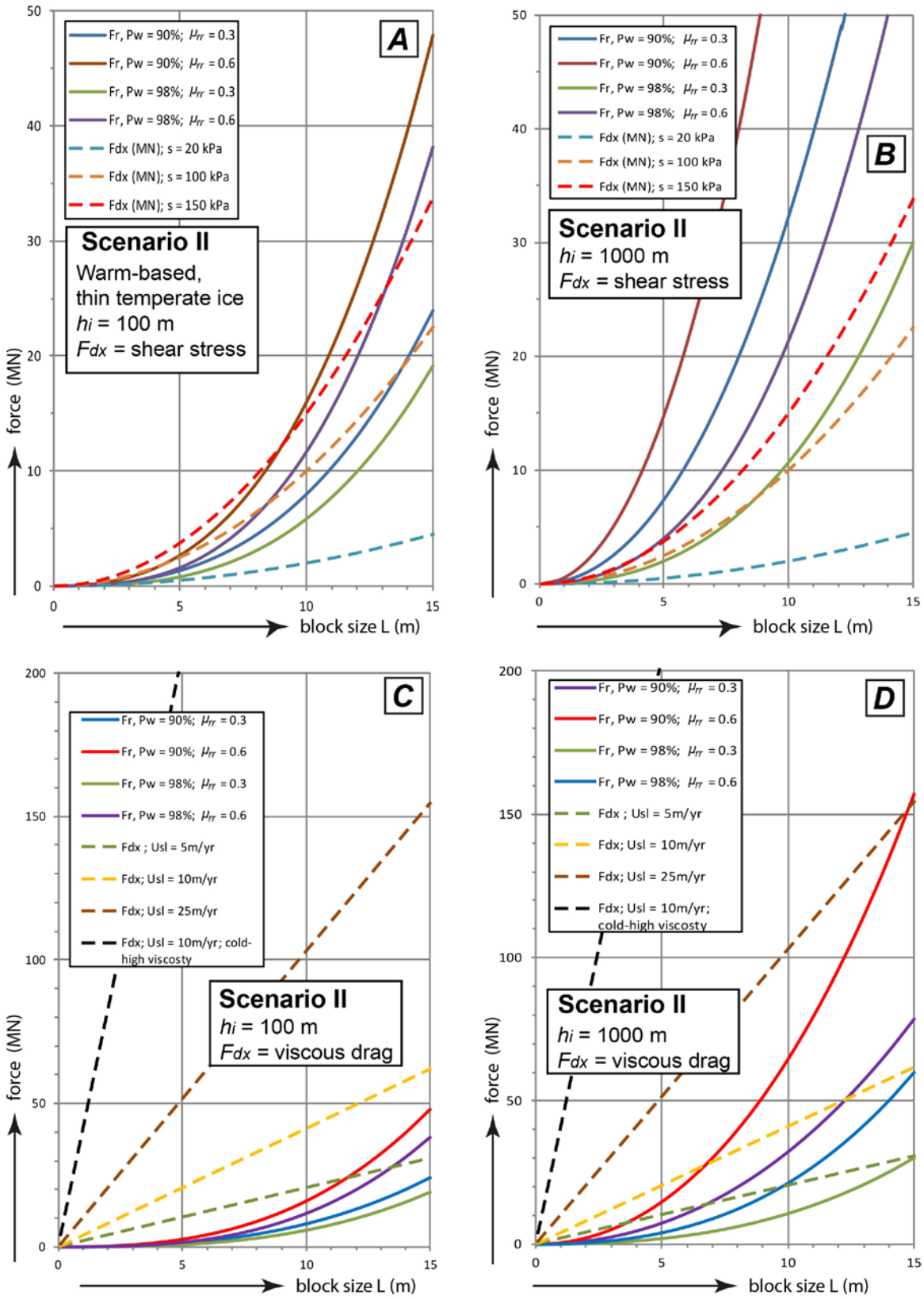

Figure 5-2. *Driving forces (dashed lines) versus resisting forces (solid lines) (in MN) as a function of block size (in m) for warm-based, thin temperate ice Scenario II. (A) using driving force calculated from shear stress, ice thickness = 100 m; (B), as (a), ice thickness = 1 000 m; (C) using driving force calculated with Stoke's Law, with different sliding velocities, with a cold-ice viscosity ($\eta = 1.3 \times 10^{12}$ Pa s), and one example of a stiffer viscosity ('cold-high viscosity'; $\eta = 1.3 \times 10^{13}$ Pa s). S = shear stress; Usl = basal sliding viscosity.*

5.4 Warm-based ice – thick temperate layer Scenario III: Driving forces and block removal

In the warm-based scenarios, the joint below the block is thawed, so we use relatively low friction coefficients (μ_{rr} = 0.3–0.6) along the basal joint. We model the driving force as generated by viscous drag, and separately, if generated by a high basal shear stress, generated by high basal melt rates (see Cohen et al. 2005).

In the case of a thick temperate ice layer, the driving force generated by viscous drag has been modelled with a temperate-ice viscosity. The results (Figure 5-3) show that block removal is more likely under thin ice than under thick ice; less likely at lower water pressures (which confusingly is more likely under thin ice, near the terminus), and in essence linearly dependent on basal sliding velocity. Because the driving forces increase linearly with block size, whereas the resisting forces increase exponentially, there is a strong sorting effect: smaller blocks are much more likely to be removed than larger blocks. (Note: this sorting effect is a consequence of the use of Stoke's law, which may be inappropriate). In the case of ice streaming (high sliding velocities and high water pressures) almost all blocks are removed, regardless of size (Figure 5.3; e.g. green dashed line and green solid line). At medium sliding velocities (50–100 m yr^{-1}) and/or low water pressures there is a strong sorting effect: larger blocks stay in place whereas smaller blocks (< 5 m) are removed.

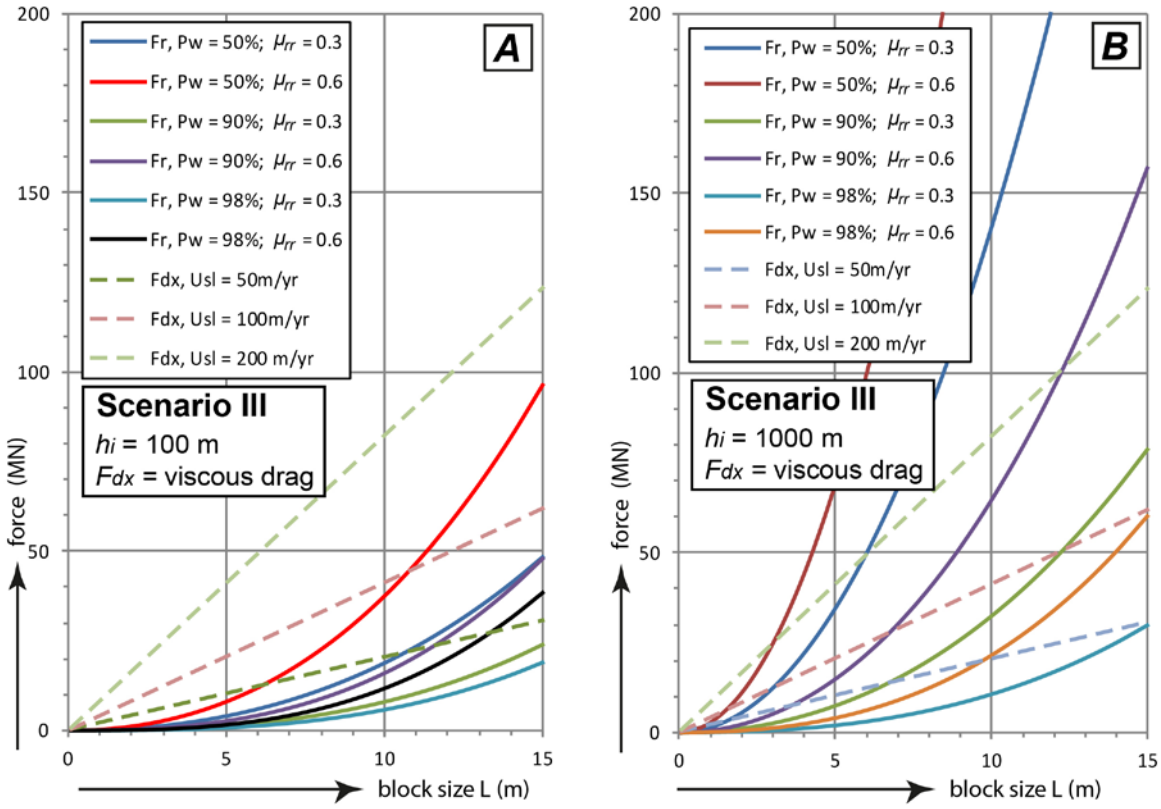

Figure 5-3. *Driving forces (dashed lines) versus resisting forces (solid lines) (in MN) as a function of block size (in m) for warm-based, thick temperate layer Scenario III, using driving force calculated with Stoke's Law, with a temperate ice viscosity ($\eta = 1.3 \times 10^{11}$ Pa s), and ice velocities of 50, 100 and 200 m yr^{-1} . (A) ice thickness of 100 m; (B) ice thickness of 1 000 m.*

In the case of high basal melting rates, high basal shear stresses may develop; in subglacial experiments below Svartisen Glacier in Norway, Cohen et al. (2005) report basal shear stresses of up to 500 kPa under c. 210 m of ice with a melt rate of 0.1–0.2 m yr^{-1}. As debris may be pressed onto the stoss, the top and both lateral side, and create high basal shear stresses on all these surfaces, we apply Equation 5-3 to calculate the basal shear stresses for this case (Figure 5-4).

The results show that in the case of high basal shear stresses (100, 200, 500 kPa) caused by high basal melt rates, block removal occurs under all circumstances. High basal melting rates in nature are unlikely to be caused by high geothermal heat flow: typical geothermal heat flows only result in melt rates of 0.01–0.1 m yr^{-1} (Cohen et al. 2005, Krabbendam 2016). Thus, to achieve the high basal melt rates to cause the high basal shear stresses, high ice velocities are required, so the situation described here are only likely in ice-stream-like scenarios. However, how this scenario can be reconciled with the low shear stresses that are derived from low-angle slopes from present-day ice-streams (e.g. Jezek et al. 2013; see Section 5.1) remains unclear.

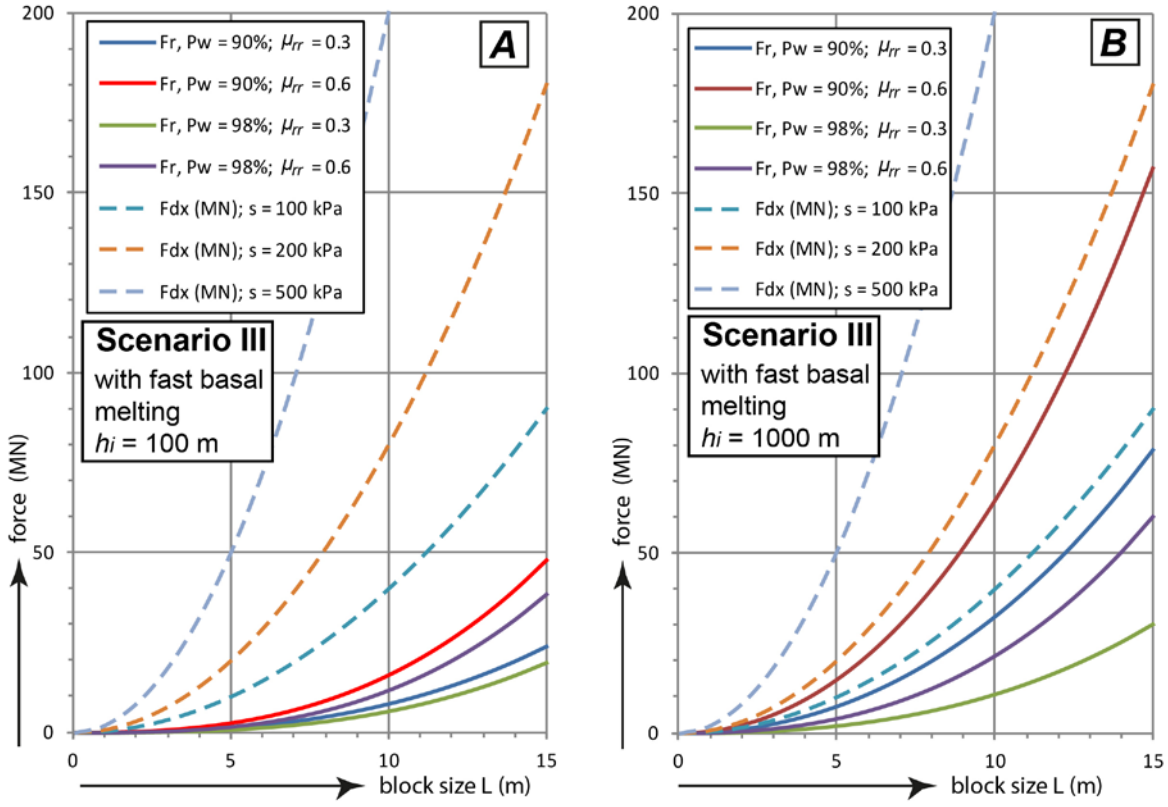

Figure 5-4. *Driving forces (dashed lines) versus resisting forces (solid lines) (in MN) as a function of block size (in m) for warm-based, thick temperate layer Scenario III, using driving force calculated from high overall basal shear stress caused by high basal melting rates – see Cohen et al. (2005). Shear stresses used are: 100, 200, 500 kPa). (A) ice thickness of 100 m; (B) ice thickness of 1 000 m.*

5.5 Freeze-on Scenario IV: Driving forces and block removal

In the freeze-on scenario (Figure 2-1), the base of the ice becomes frozen to the block and, as in the cold-based scenario, we derive the driving force from the applied basal shear stress, with ice frozen onto the stoss side as well as the top- and lateral sides (Equation 5-3). Ice-flow velocities are low, but as the ice is frozen to its base and has a high viscosity, driving stress may be high. However, it is possible that the contact between the block and its substrate (the basal joint) is thawed, with associated relatively low friction coefficients (μ_{rr} = 0.3–0.6). Note that for this situation to occur the 0 °C isotherm must occur just below the ice-bed contact, in essence within the block. Furthermore, because basal melting, surface melting and possibly supraglacial lake drainage events may occur up-ice, high water pressures may build up, with water trying to escape below the frozen boundary within the substrate (e.g. Piotrowski 2006). If this situation occurs, it is likely to do so close to the glacier terminus: here the steeper slope leads to a steep water pressure gradient. Altogether this may lead to high water pressures near the ice-bed; indeed overpressure ($P_w > P_i$) is possible, even if only intermittently (see also Boulton et al. 2001, Claesson Liljedahl et al. 2016).

The results (Figure 5-5) show that block removal is highly likely if driving stresses are > 20 kPa, and water pressures are high (≥ 90 %). If the driving stresses are > 50 kPa (brown dashed line in Figure 5-4), block removal is possible even at relatively high friction coefficient at the base and with water pressures of 90 %. As in the case of cold-based ice, the curves of the resisting and driving forces are subparallel so there is no strong dependency on block size.

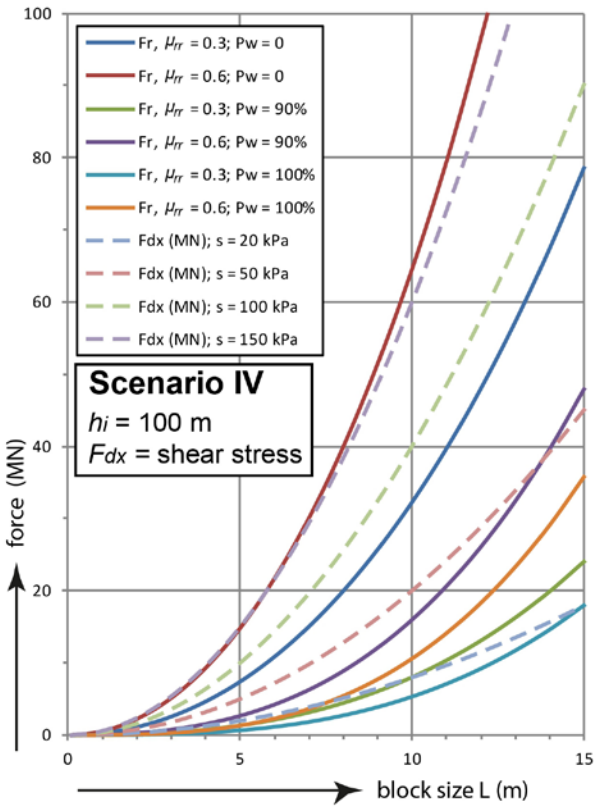

Figure 5-5. *Driving forces (dashed lines) versus resisting forces (solid lines) (in MN) as a function of block size (in m) for 'freeze-on' Scenario IV, using driving force calculated from the overall shear stress (s = 20, 50, 100, 150 kPa).*

6 Effect of block shape and streamlining

Thus far, we have only considered cubic blocks, which is reasonable when considering removal of tors. However, geomorphological studies of hard, warm-based glaciated terrains have shown that more streamlined, non-cubic bedforms (whalebacks, roches moutonnées) are common (e.g. Rastas and Seppälä 1981, Krabbendam and Bradwell 2014) and this is also to be the case in the Forsmark area (Figure 1-1; Hall et al. 2019), whereas hard palaeo ice-stream beds are highly streamlined, with few, if any, blunt upstanding rocks present (e.g. Bradwell 2013, Krabbendam et al. 2016). Here, we explore three different block geometries. Firstly, we look at flattened cuboids ('slabs') with a square top area, but variable height (Figure 6-1 A). Secondly we look at elongate cuboids (akin to whalebacks or rock ridges), with a square stoss side, but variable length (Figure 6-1 B). Thirdly we look at streamlining, mimicked here by varying the slope of the stoss side on an elongate cuboid (Figure 6-1 C).

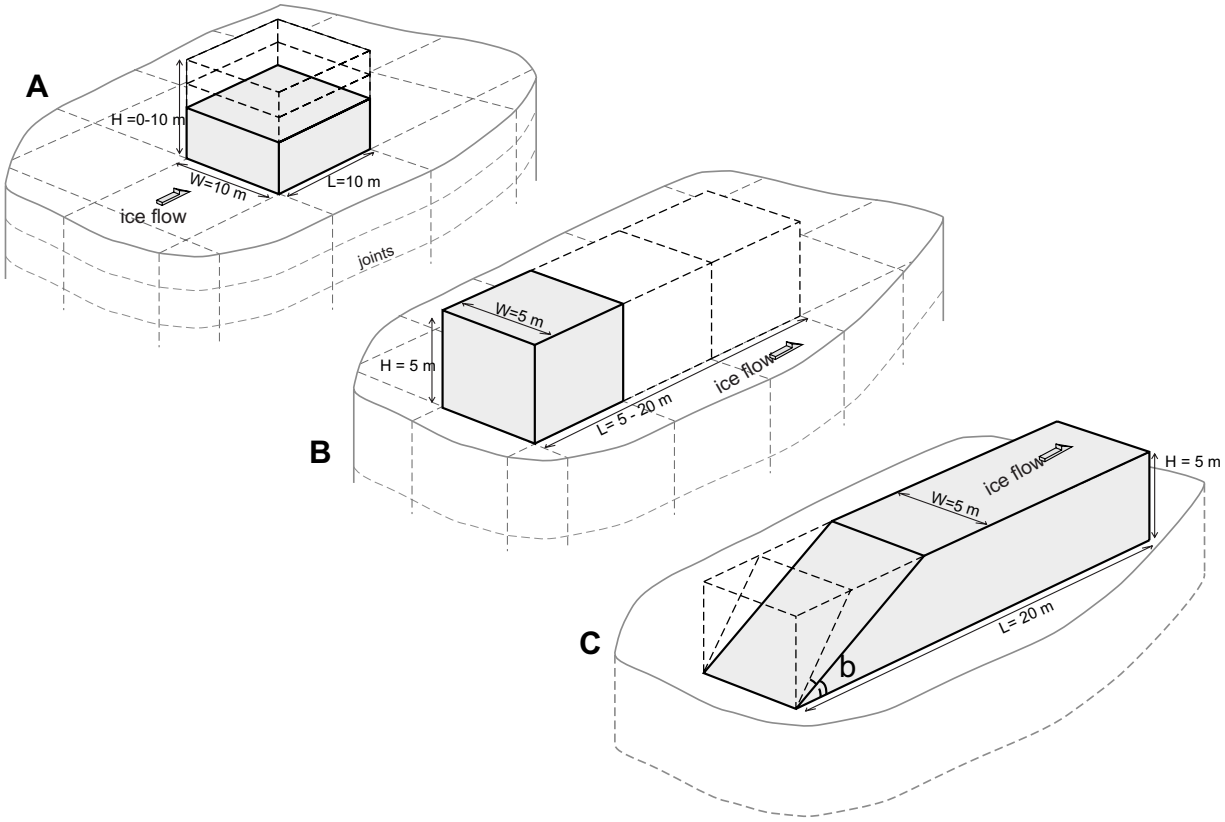

Figure 6-1. *Schematic drawing showing geometry of block with non-cubic shape. (A) Flat cuboid, with square top surface area, but variable height. (B) Elongate cuboid, with square stoss-side, but variable length, along the ice-flow direction. (C) Elongate cuboid, with sloping stoss side.*

6.1 Warm-based ice – thick temperate ice Scenario III: Effect of block shape and streamlining

We first explore non-cubic block shapes for the warm-based, thick temperate ice Scenario III, with an ice thickness of 1 000 m, a sliding velocity of 100 and 200 m yr^{-1}, in the case of a block with a top surface of 10 × 10 m, but height *H* varying from 10 to 0 m (Figure 6-1 A).

The buoyant weight of a non-cubic block is given by:

$$F_{bz} = L\,W\,H\,(\rho_r - \rho_w)g \text{ (in N)} \quad (6\text{-}1)$$

where L, W and H are the length, width and height of the block respectively. The weight of the overlying ice exerted on a non-cubic block is given by:

$$F_{iz} = h_i\,g\,\rho_i\,L\,W\,P_{ref} \quad (6\text{-}2)$$

The volume of the block decreases linearly with decreasing height, and so does the buoyant weight. However, the surface area of the top remains the same, so that the normal force exerted by the weight of the ice (Equation 6-2) remains the same. As a consequence, the resisting forces remain fairly constant. The surface area of the stoss-side decreases with decreasing height, which leads to a decrease in the driving force (Equation 5-1, with $L = (H+W)/2$). Thus, the driving forces are strongly dependent on height; so that high blocks ($H > 3$–7 m) can be moved, whereas lower, flatter ('slabby') blocks remain (Figure 6-2 A).

In the case of elongate blocks (Figure 6-2 B), we vary the length of the block between 5–20 m, but with constant height and width ($H = W = 5$ m). In this case the stoss-side surface area and hence the driving force remain constant (Equation 5-1, if *W* is used instead of *L*, see horizontal lines on Figure 6-2 B), but the resisting force varies linearly with the length because both the volume and the top surface vary linearly with the length (Equations 6-1 and 6-2). The result is that with increasing elongation (greater length in the plot) there is significantly lower probability of block removal.

The effect of true streamlining is mimicked by varying the slope of the stoss-side. As streamlining for laminar flow is less well studied than for turbulent flow, we take the relatively simple approach that the viscous drag on the stoss side decreases linearly with the sin of the slope β of the stoss side:

$$F_d \approx \sin\beta\; 10\; H\,\eta\,U_{sl} \quad (6\text{-}3)$$

where *H* is the height of the obstacle, η the ice viscosity and U_{sl} the sliding velocity. We calculate this for an obstacle with a height and width of 5 m, a length of 20 m, under 1 000 m of ice, with a sliding velocity of 200 m yr^{-1}. On Figure 6-2 C is clear that streamlining does have a significant effect, with block removal becoming less likely once the stoss side slope drops below 40–60°.

The above situations are quite intuitive and consistent with the observations of elongate and flat blocks remaining on the beds of palaeo-ice streams. The streamlining itself is likely to be caused by abrasion, or lateral plucking (Krabbendam and Bradwell 2011), which is not further discussed herein.

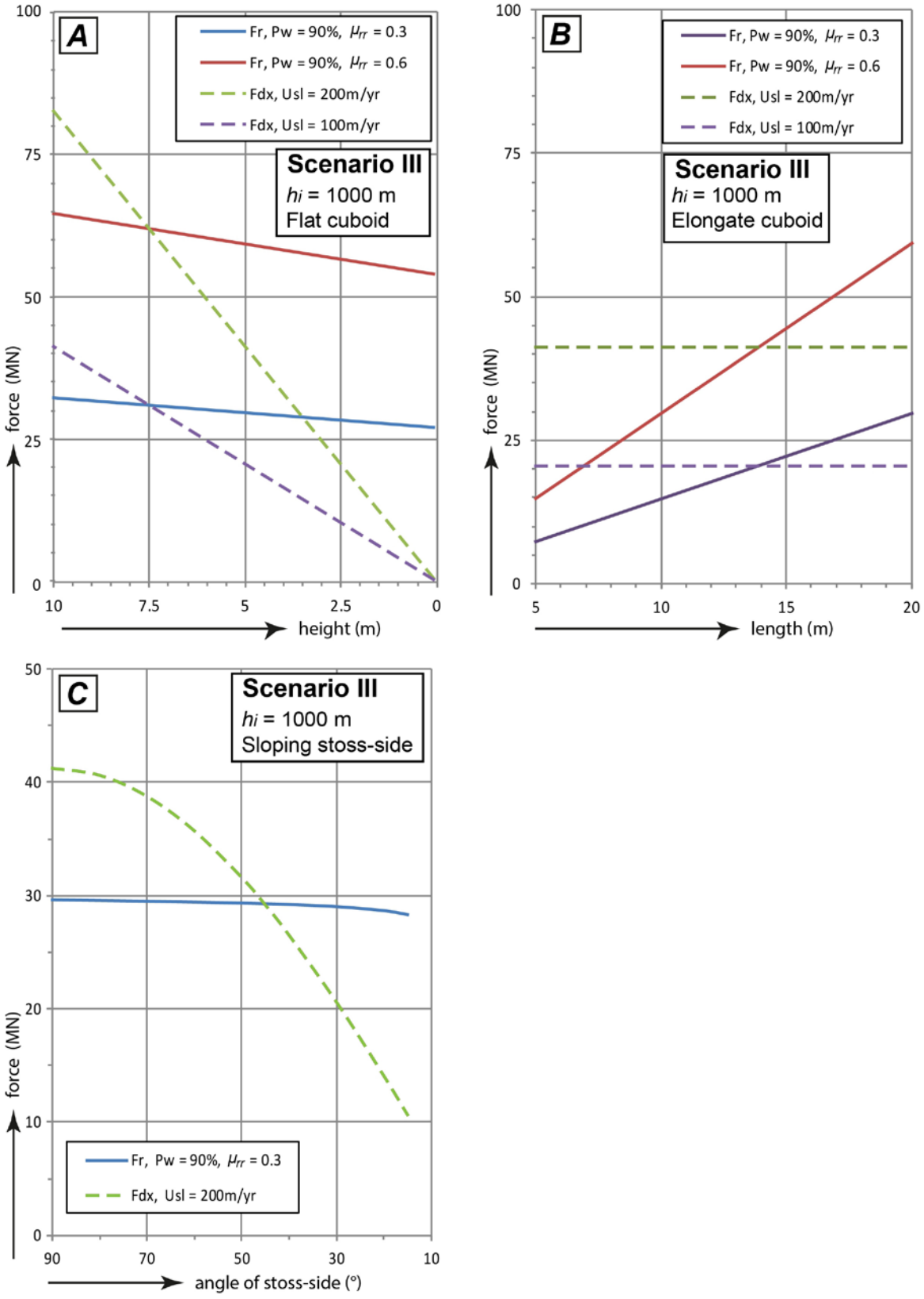

Figure 6-2. *The effect of block shape on the balance of driving forces (dashed lines) versus resisting forces (solid lines) (in MN) for warm-based, thick temperate ice Scenario III. Balance of forces for (A) flat cuboid, with length and width set at 10 m, but varying height between 0–10 m (horizontal axis); (B) elongate cuboid, with height and width set at 5 m, but length (along ice flow) varying between 5–20 m (horizontal axis); (C) elongate cuboid with sloping stoss side, as a function of stoss-side slop (in °, horizontal axis). Driving force calculated with Stoke's Law, with a temperate ice viscosity (η = 1.3 × 10^{11} Pa s); ice height is 1 000 m; water pressure is 90 %.*

6.2 Freeze-on Scenario IV: Effect of block shape

We also explore the effect of block shape for the freeze-on Scenario IV, with an ice thickness of 100 m, and water pressures of 90 % and 100 %. We use the same geometries as in Figure 6-1 and show the case of a flat cuboid with a length and width of 10 m, but varying height from 10 to 0 m (Figure 6-3 A); and the case of an elongate cuboid with a height and width of 5 m, but varying length from 5 to 20 m (Figure 6-3 B). It appears that block shape has little effect: removal occurs at medium to high shear stresses (50–100 kPa), almost regardless of block shape. This is because the ice is frozen onto the block, the shear stress not only acts onto the stoss-side, but also on the top and lateral sides (see Section 5.1), and this surface area increases linearly with height (or length). As a result, the driving forces increase at a similar rate as the resisting forces. Thus, whereas block shape has a major effect at a warm-base, it has little or no effect during the freeze-on scenario. Put another way, during the freeze-on scenario slabby and elongate cuboids have as much probability to be removed as more cubic blocks, whereas under warm-based sliding such streamlined forms have a much higher preservation potential.

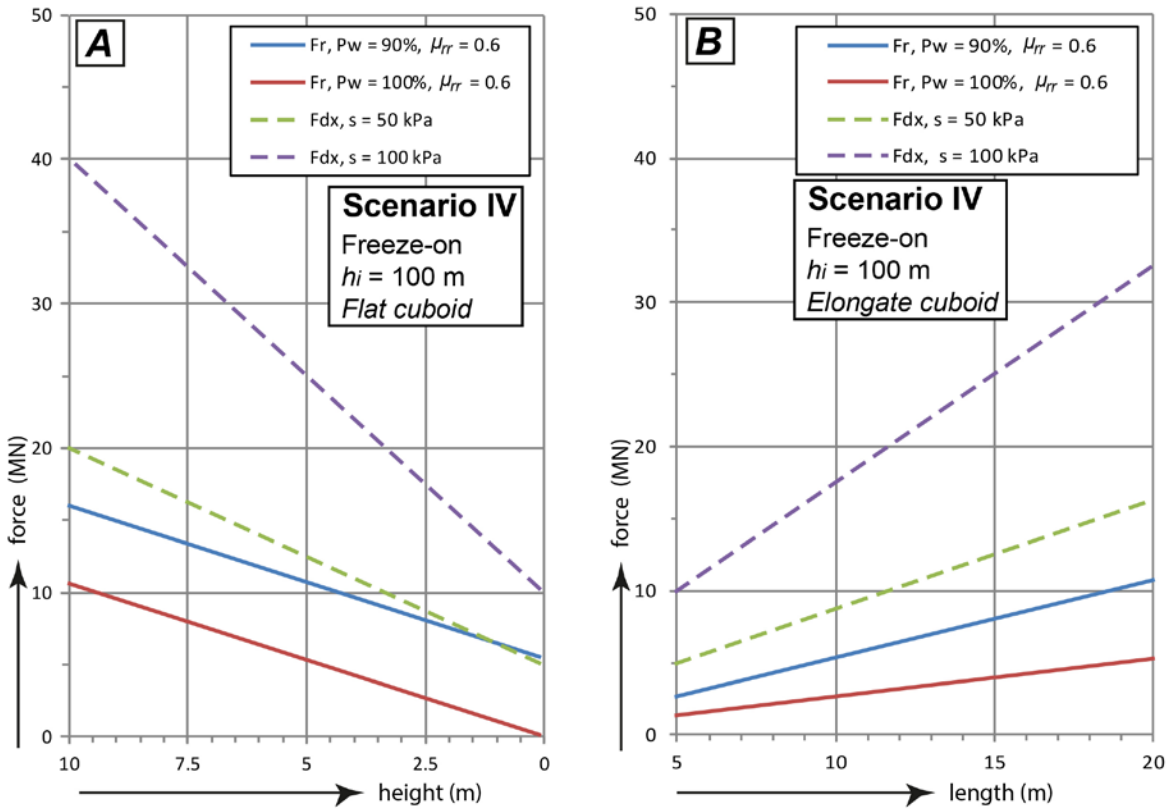

Figure 6-3. *Driving forces (dashed lines) versus resisting forces (FR – solid lines) (in MN) for freeze-on Scenario IV, using driving force calculated from the shear stress F_{dx} acting on the stoss side as well as the top and lateral sides; ice height at 1 000 m; and water pressure of 90 % and 100 %. (A) Balance of forces for flat cuboid, with length and width set at 10 m, but varying height between 0–10 m (horizontal axis). (B) Balance of forces for elongate cuboid, with height and width set at 5 m, but varying length (along ice flow) varying between 5–20 m (horizontal axis).*

7 Discussion

7.1 Consistent outcomes

Despite a number of uncertainties discussed below, a number of consistent outcomes and preliminary conclusions are apparent.

Overall, one perhaps surprising conclusion is that block removal is more likely beneath thin ice than under thick ice under all three scenarios for which this was calculated (cold-based and warm-based scenarios). The reason behind this is that the weight of the ice, which is linearly dependent on ice thickness, is a significant contributing factor to the resisting force, so that resisting forces increase faster with ice thickness than the driving forces.

Under **cold-based conditions**, block removal is not likely (Figure 5-1). The resisting forces are high, because there is no water pressure, and the friction-coefficient between the block and the bed are high. In contrast, the driving forces are probably fairly low. Only in the case of very high driving stresses (> 150 kPa), thin ice and relatively low friction coefficient, block removal may occur, but such conditions may not be realistic in nature. In a review of the thermal state of the base of the Greenland Ice Sheet MacGregor et al. (2016) showed that in those areas where the base is frozen, the basal stresses are below c. 70 kPa. If block removal occurs, there is little dependency on block size, since the curves of driving and resisting forces are near parallel. In simple terms: either all blocks stay or all blocks move and there is no significant 'sorting' effect at least up to maximum block lengths of 15 m.

In the **warm-based thin temperate ice scenario**, the resisting forces are much lower than under cold-based ice, because water pressure is likely to be high (modelled here at ≥ 90 % of overburden pressure as observed from the Greenland Ice Sheet.). The results are somewhat contradictory between the basal shear stress and the viscous drag. If the driving forces are calculated using the basal shear stress, block removal is only likely at high shear stresses and thin ice (Figure 5-2 A and B). Such conditions may possibly occur during the growth of an ice sheet and the temporal change from cold-to-warm based conditions. On the other hand, if the forces are dependent on viscous drag around the obstacle, than block removal is significantly more likely, and specifically so for small blocks than for larger ones (Figure 5-2 C and D), suggesting a significant sorting effect. Whether or not block removal occurs by viscous drags depends strongly on the ice viscosity, which is poorly constrained.

In the **warm-based, thick temperate ice scenario**, block removal is likely, but depends largely on water pressure and ice sliding velocity (Figure 5-3). At high basal sliding velocities (e.g. around and above 200 m yr^{-1}) and high water pressures, as likely beneath an ice stream, all blocks are removed. At intermediate basal sliding velocities (e.g. 50–100 m yr^{-1}) and low water pressures, as found near the terminus of the GAP area for instance, only small blocks are removed, and a pronounced sorting effect is likely.

The case of high basal shear stresses, caused by high basal melting rates (e.g. Cohen et al. 2005) block removal is highly likely under most conditions (Figure 5-3). However, the high basal shear stresses are at odds with those derived from present-day ice sheets, so it is uncertain how realistic these situations are.

It should be noted that the strong 'sorting effect' as seen for both warm-based scenarios is the result of the application of Stoke's Law, wherein the driving force increases linearly rather than exponentially with block size. If viscous drag would be modelled with a general viscous drag equation (see Section 7.3), the sorting effect may be less.

We further note that under fast-flowing ice, abrasion is also an important erosion mechanism, as abrasion rate is likely to be strongly dependent on sliding velocity (e.g. Glasser and Bennett 2004). Abrasion has not been discussed herein.

Block shape and streamlining are important under fast-flowing ice (Figure 6-2). A flat cuboid ('slab') has a much lower driving force applied to it than a cubic block, whereas an elongate cuboid has a much higher resisting force: in either case they have significantly less probability of moving than cubic tors. Equally, a sloping ('streamlined') stoss-side decreases the driving force applied to the block and lowers

the probability of removal. These conclusions are consistent with geomorphological observations of streamlined bedrock features (rock ridges, roches moutonnées, whalebacks etc.) preserved beneath areas of presumed fast palaeo-ice flow (e.g. Bradwell 2013). Specifically, the conclusions are applicable to the low amplitude, high wavelength bedrock forms at Forsmark.

In the **freeze-on scenario**, the top of the block becomes frozen onto the overlying ice, whereas the base of block may remain thawed. This scenario is highly effective in block removal, particularly if accompanied by high water pressure ($P_w > 90$ %). Even at relatively modest driving stresses (50 kPa), almost all blocks are removed at such a water pressure (Figure 5-4). There is little or no sorting effect: larger blocks have almost the same chance of removal as smaller ones. Block shape and streamlining are not very relevant for the freeze-on scenario: more streamlined blocks have as much probability of moving as cubic, blunt block (Figure 6-3). This is basically because if freeze-on conditions occur, the frozen bed affects the entire top surface of the block, and is thus independent of block shape. However, the 'freeze-on' scenario is to an extent a rather special case. The relatively rarity of glacial rafts, especially of crystalline rock (Talbot 1999), and the fact that not all glacial rafting may be caused by freeze-on (e.g. Ruszcyńska-Szenajh 1987), would suggest that the freeze-on scenario is, in nature, relatively rare.

7.2 Transient and ice-frontal scenarios

In this analysis, each scenario is treated as a steady state scenario. In reality, over a glacial cycle, any one location may change from one scenario to another, possibly multiple times for instance during glacial re-advances. The boundary of cold-to-warm based conditions is also likely to vary in space and time. As an example, upstanding tors with negligible glacial modification on the Cairngorm plateau in Scotland occur at elevation only slightly above glacially modified tors, 'stumps' or 'plinths' suggestive of wholesale tor removal, which in turn pass at lower elevations into asymmetric roche moutonnée forms (Hall and Glasser 2003, Hall and Phillips 2006). The variable modification of the tors may well be caused by local variations of the englacial cold-warm boundary in space and time. These transitions have not been modelled herein, but we note that the temporal change from cold-to-warm based conditions may well result in transient high shear stresses. Similarly, the transition from warm-based to freeze-on may be characterised by high water pressures. Either set of conditions may develop as ice thins during deglaciation.

It is stressed here that the situation at the actual front of a glacier or ice sheet during a glacial advance, i.e. that give rise to push moraines and similar ice-marginal deposits, has not been modelled in this report, as it requires a very different approach. It is possible that this situation is highly likely to lead to block removal.

7.3 Uncertainties

The normal forces acting on the base of the block are probably fairly well constrained. In practice, the main uncertainty will be the magnitude of water pressures, as these can vary strongly, specifically in ice-marginal locations. Concerning the resisting forces, a major uncertainty lies in the estimation of the effective friction coefficient along the basal joint. This uncertainty stems mainly from natural variation of joint surfaces, such as presence of asperities, cementation or granular material. It is possible that more is known from the engineering geology literature.

Larger uncertainties exist with the estimation of the driving forces. Firstly, it is uncertain whether it is the basal shear stress (Equation 5-2) or Stoke's Law (Equation 5-1) that is most appropriate. Here, we have taken the approach that the shear stress is most appropriate under low ice sliding velocities, and Stoke's Law under high sliding velocities. However, under the warm-based scenario, both high and low sliding velocities are possible. Applied to similar situations under the warm-based scenario, the results are rather different, and it is in this scenario that the choice of correct formulation of driving forces is most important (Figure 5-2).

Furthermore, it is uncertain whether or not Stoke's Law is applicable in the first place for ice flow around large obstacles. In general, Stoke's Law is applicable to laminar flow, with low Reynolds numbers. Reynolds numbers for ice flow are exceedingly low ($\mathrm{Re} \sim 7.7 \times 10^{-11}$, or smaller; see Appendix 2),

so according to this measure Stoke's Law should be valid. Stoke's Law has been empirically validated for situations of low-medium viscosity fluids (water, blood) flowing past very small objects (clay or silt particles) or through very narrow pipes (e.g. capillary veins). However, no literature was found dealing with the empirical validity (or invalidity!) of large, metre-scale objects in a very high viscosity medium like ice. The problem is that in Stoke's Law, the forces increase linearly with the length of a block (or the radius of a sphere), rather than the surface area: this may simply be an approximation that is valid at small scales, but not for large, metre-scale obstacles. It is thus uncertain whether or not Stoke's Law is applicable to the scenario of a large rock obstacle in ice flow. This affects the warm-based scenarios, modelled for viscous drag (Figures 5-2 C, D; 5-3). It may be recommended for future modelling to apply a general viscous drag equation.

Further uncertainties exist concerning the viscosity of ice. It is shown that the probability of block removal by viscous drag is strongly dependent on ice viscosity. This would be the case regardless of whether Stoke's Law or a general viscous drag equation would be used. Whilst the rheological behaviour of cold ice is well understood (Glen 1955, Alley 1992, Cuffey and Paterson 2010) and has been tested empirically by tilt meters in boreholes in ice sheets (e.g. Ryser et al. 2014, Lüthi et al. 2002), the effective viscosity is highly variable and strongly dependent in a non-linear manner on the locally applied deviatoric stress as well as temperature. These parameters, in turn, are very difficult to reconstruct for the Fennoscandian Ice Sheet. For temperate ice, ice viscosity is uncertain for other reasons. Because the temperature is set at a singular value (the pressure-melting point) there is no temperature dependence. However, the actual rheological behaviour is poorly constrained, with high uncertainty as to the value of the stress exponent (n): some authors suggest $n \sim 3$, others $n \sim 1$; others suggest that the value of n may vary between $n = 1$ to 4 depending on the stress (Colbeck and Evans 1973, Chandler et al. 2008, Byers et al. 2012; see discussion in Krabbendam 2016). Many reviews of ice rheology simply ignore the problem of temperate ice rheology altogether (Budd and Jacka 1989, Alley 1992), although it appears widely accepted that temperate ice is weaker (lower viscosity) than cold ice, in part as a function of water content (Duval 1977).

7.4 Potential future steps

We have here simplified the problem of calculating the forces required to move an upstanding block of bedrock beneath an ice sheet. Next steps could involve extension of the scope of the modelling, reduction of uncertainties and its application to known glaciated terrains:

1. We consider bedrock blocks as single cuboidal blocks 5–15 m long akin to tors or cnocs. In reality tors and cnocs may comprise multiple contiguous blocks separated by joints that form larger hills. Where cnocs have been shaped by glacial erosion to give roche moutonnée forms, the lee-side cliff is the main location for block removal (quarrying). These locations lack a stoss face and so the modelling of tractive forces is different.
2. A similar approach as used herein may be applied to glacial quarrying, which is relevant for the glacial erosion in the Forsmark area. It should be noted here that much of the older literature on quarrying (e.g. Hallet 1996) focussed on the problem of creating a fracture, whereas it is now known that glacial plucking utilises pre-existing fractures and joints (Dühnforth et al. 2010, Krabbendam and Glasser 2011, Hooyer et al. 2012).
3. Questions over the applicability of Stoke's Law (for large objects in a very viscous medium) may be addressed by numerical modelling or possibly by analysing present-day ice flow over rough, hard beds with known subglacial topography. In future modelling, it is recommended to apply a general viscous drag equation to judge whether this alleviates the uncertainty surrounding the application of Stoke's law.
4. The modelling predicts block removal at a late stage of deglaciation when ice is thin and hydraulic pressures may be temporarily high. This situation may account for the block-rich tills found around Forsmark that have been transported only for short distances, but this would require further testing.

Acknowledgements

Andrew Finlayson is thanked for comments on earlier versions of this report. Joel Harper and Jens-Ove Näslund are thanked for thorough but constructive reviews of this report.

References

SKB's (Svensk Kärnbränslehantering AB) publications can be found at www.skb.com/publications.

Alley R, 1992. Flow-law hypotheses for ice-sheet modelling. Journal of Glaciology 38, 245–256.

Aschwanden A, Blatter H, 2005. Meltwater production due to strain heating in Storglaciären, Sweden. Journal of Geophysical Research 110, F04024. doi:10.1029/2005JF000328

Aschwanden A, Bueler E, Khroulev C, Blatter H, 2012. An enthalpy formulation for glaciers and ice sheets. Journal of Glaciology 58, 441–457.

Beckholmen M, Tirén S A, 2009. The geological history of the Baltic Sea, a review of the literature and investigation tools. Stockholm: Swedish Radiation Safety Authority. (SSM 2009:21)

Boulton G S, 1979. Processes of glacier erosion on different substrata. Journal of Glaciology 23, 15–38.

Boulton G S, Dobbie K E, Zatsepin S, 2001. Sediment deformation beneath glaciers and its coupling to the subglacial hydraulic system. Quaternary International 86, 3–28.

Bradwell T, 2013. Identifying palaeo-ice-stream tributaries on hard beds: Mapping glacial bedforms and erosion zones in NW Scotland. Geomorphology 201, 397–414.

Brinkerhoff D J, Meierbachtol T W, Johnson J V, Harper J T, 2011. Sensitivity of the frozen/melted basal boundary to perturbations of basal traction and geothermal heat flux: Isunnguata Sermia, western Greenland. Annals of Glaciology 52, 43–50.

Budd W F, Jacka T H, 1989. A review of ice rheology for ice sheet modelling. Cold Regions Science and Technology 16, 107–144.

Budd W F, Keage P L, Blundy N A, 1979. Empirical studies of ice sliding. Journal of Glaciology 23, 157–170.

Byers J, Cohen D, Iverson N R, 2012. Subglacial clast/bed contact forces. Journal of Glaciology 58, 89–98.

Chandler D, Hubbard B, Hubbard A, Murray T, Rippin D, 2008. Optimising ice flow law parameters using borehole deformation measurements and numerical modelling. Geophysical Research Letters 35, L12502. doi: 10.1029/2008GL033801

Claesson Liljedahl L, Kontula A, Harper J, Näslund J-O, Selroos J-O, Pitkänen P, Puigdomenech I, Hobbs M, Follin S, Hirschorn S, Jansson P, Kennell L, Marcos N, Ruskeeniemi T, Tullborg E-L, Vidstrand P, 2016. The Greenland Analogue Project: Final report. SKB TR-14-13, Svensk Kärnbränslehantering AB.

Cohen D, Iverson N R, Hooyer T S, Fischer U H, Jackson M, Moore P L, 2005. Debris-bed friction of hard-bedded glaciers. Journal of Geophysical Research 110, F02007. doi:10.1029/2004JF000228

Colbeck S C, Evans R J, 1973. A flow law for temperate glacier ice. Journal of Glaciology 12, 71–86.

Cuffey K M, Paterson W S B, 2010. The physics of glaciers. 4th ed. Burlington, MA: Butterworth-Heinemann/Elsevier.

Dahl-Jensen D, 1989. Steady thermomechanical flow along two-dimensional flow lines in large grounded ice sheets. Journal of Geophysical Research 94, 10355–10362.

Duval P, 1977. The role of the water content on the creep rate of polycrystalline ice. IAHS Publication 118, 29–33.

Dühnforth M, Anderson R S, Ward D, Stock G M, 2010. Bedrock fracture control of glacial erosion processes and rates. Geology 38, 423–426.

Fahnestock M, Abdalati W, Joughin I, Brozena J, Gogineni P, 2001. High geothermal heat flow, basal melt, and the origin of rapid ice flow in central Greenland. Science 294, 2338–2342.

Forssberg O, Mærsk Hansen L, Koyi S, Vestgård J, Öhman J, Petersson J, Albrecht J, Hedenström A, Gustavsson J, 2007. Forsmark site investigation. Detailed fracture and bedrock mapping, Quaternary investigations and GPR measurements at excavated outcrop AFM001264. SKB P-05-269, Svensk Kärnbränslehantering AB.

Furbish D J, 1997. Fluid physics in geology: An introduction to fluid motions on Earth's surface and within its crust. New York: Oxford University Press.

Glen J W, 1955. The creep of polycrystalline ice. Proceedings of the Royal Society of London. Series A. Mathematical and Physical Sciences 228, 519–538.

Glasser N F, Bennett M R, 2004. Glacial erosional landforms: origins and significance for palaeoglaciology. Progress in Physical Geography 28, 43–75.

Hall A M, Glasser N F, 2003. Reconstructing the basal thermal regime of an ice stream in a landscape of selective linear erosion: Glen Avon, Cairngorm Mountains, Scotland. Boreas 32, 191–207.

Hall A M, Phillips W M, 2006. Glacial modification of granite tors in the Cairngorms. Scotland. Journal of Quaternary Science 21, 811–830.

Hall A M, Ebert K, Goodfellow B W, Hättestrand C, Heyman J, Krabbendam M, Moon S, Stroeven A P, 2019. Past and future impact of glacial erosion in Forsmark and Uppland, Sweden. SKB TR-19-07, Svensk Kärnbränslehantering AB.

Hallet B, 1979. A theoretical model of glacial abrasion. Journal of Glaciology 23, 39–50.

Harper J, Hubbard A, Ruskeeniemi T, Claesson Liljedahl L, Kontula A, Hobbs M, Brown J, Dirkson A, Dow C, Doyle S, Drake H, Engström J, Fitzpatrick A, Follin S, Frape S, Graly J, Hansson K, Harrington J, Henkemans E, Hirschorn S, Humphrey N, Jansson P, Johnson J, Jones G, Kinnbom P, Kennell L, Klint K E S, Liimatainen J, Lindbäck K, Meierbachtol T, Pere T, Pettersson R, Tullborg E-L, van As D, 2016. The Greenland Analogue Project: Data and Processes. SKB R-14-13, Svensk Kärnbränslehantering AB.

Harrington J A, Humphrey N F, Harper J T, 2015. Temperature distribution and thermal anomalies along a flowline of the Greenland ice sheet. Annals of Glaciology 56, 98–104.

Hooyer T S, Cohen D, Iverson N R, 2012. Control of glacial quarrying by bedrock joints. Geomorphology 153–154, 91–101.

Hättestrand C, Stroeven A P, 2002. A relict landscape in the centre of Fennoscandian glaciation: Geomorphological evidence of minimal Quaternary glacial erosion. Geomorphology 44, 127–143.

Iken A, Echelmeyer K, Harrions W, Funk M, 1993. Mechanisms of fast flow in Jakobshavns Isbrre, West Greenland: Part I. Measurements of temperature and water level in deep boreholes. Journal of Glaciology 39, 15–25.

Iverson N R, Cohen D, Hooyer T S, Fischer U H, Jackson M, Moore P L, Lappegard G, Kohler J, 2003. Effects of basal debris on glacier flow. Science 301, 81–84.

Jaquet O, Namar R, Siegel P, Jansson P, 2012. Groundwater flow modelling under ice sheet conditions in Greenland (phase II). SKB R-12-14, Svensk kärnbränslehantering AB.

Jezek K, Wu X, Paden J, Leuschen C, 2013. Radar mapping of Isunnguata Sermia, Greenland. Journal of Glaciology 59, 1135–1146.

Kleman J, 1994. Preservation of landforms under ice sheets and ice caps. Geomorphology 9, 19–32.

Kleman J, Hättestrand C, Borgström I, Stroeven A, 1997. Fennoscandian palaeoglaciology reconstructed using a glacial geological inversion model. Journal of Glaciology 43, 283–299.

Kleman J, Stroeven A P, Lundqvist J, 2008. Patterns of Quaternary ice sheet erosion and deposition in Fennoscandia and a theoretical framework for explanation. Geomorphology 97, 73–90.

Krabbendam M, 2016. Sliding of temperate basal ice on a rough, hard bed: creep mechanisms, pressure melting, and implications for ice streaming. The Cryosphere 10, 1915–1932.

Krabbendam M, Bradwell T, 2011. Lateral plucking as a mechanism for elongate erosional glacial bedforms: explaining megagrooves in Britain and Canada. Earth Surface Processes and Landforms 36, 1335–1349.

Krabbendam M, Bradwell T, 2014. Quaternary evolution of glaciated gneiss terrains: pre-glacial weathering vs. glacial erosion. Quaternary Science Reviews 95, 20–42.

Krabbendam M, Glasser N F, 2011. Glacial erosion and bedrock properties in NW Scotland: Abrasion and plucking, hardness and joint spacing. Geomorphology 130, 374–383.

Krabbendam M, Eyles N, Putkinen N, Bradwell T, Arbeleaz-Moreno L, 2016. Streamlined hard beds formed by palaeo-ice streams: A review. Sedimentary Geology 338, 24–50.

Krabbendam M, Bradwell T, Everest J D, Eyles N, 2017. Joint-bounded crescentic scars formed by subglacial clast-bed contact forces: implications for bedrock failure beneath glaciers. Geomorphology 290, 114–127.

Lagerbäck R, Sundh M, Svedlund J-O, Johansson H, 2005. Forsmark site investigation. Searching for evidence of late- or postglacial faulting in the Forsmark region. Results from 2002–2004. SKB R-05-51, Svensk Kärnbränslehantering AB.

Lidmar-Bergström K, Bonow J M, Japsen P, 2012. Stratigraphic Landscape Analysis and geomorphological paradigms: Scandinavia as an example of Phanerozoic uplift and subsidence. Global and Planetary Change 100, 153–171.

Lüthi M, Funk M, Iken A, Gogineni S, Truffer M, 2002. Mechanisms of fast flow in Jakobshavn Isbrae, West Greenland: Part III. Measurements of ice deformation, temperature and cross-borehole conductivity in boreholes to the bedrock. Journal of Glaciology 48, 369–385.

Lönnqvist M, Hökmark H, 2013. Approach to estimating the maximum depth for glacially induced hydraulic jacking in fractured crystalline rock at Forsmark, Sweden. Journal of Geophysical Research: Earth Surface 118, 1777–1791.

MacGregor J A, Fahnestock M A, Catania G A, Aschwanden A, Clow G D, Colgan W T, Gogineni S P, Morlighem M, Nowicki S M, Paden J D, 2016. A synthesis of the basal thermal state of the Greenland Ice Sheet. Journal of Geophysical Research: Earth Surface 121, 1328–1350.

Marshall S J, Clark P U, 2002. Basal temperature evolution of North American ice sheets and implications for the 100 kyr cycle. Geophysical Research Letters 29, 2214. doi: 10.1029/2002GL015192

Meierbachtol T W, Harper J T, Johnson J V, Humphrey N F, Brinkerhoff D J, 2015. Thermal boundary conditions on western Greenland: Observational constraints and impacts on the modeled thermomechanical state. Journal of Geophysical Research: Earth Surface 120, 623–636.

Meierbachtol T W, Harper J T, Humphrey N F, Wright P, 2016. Mechanical forcing on water pressure in a hydrologically isolated reach beneath Western Greenland's ablation zone. Annals of Glaciology 57, 62–70.

Morgan V I, 1991. High-temperature ice creep tests. Cold Regions Science and Technology 19, 295–300.

Näslund J-O, Jansson P, Fastook J L, Johnson J, Andersson L, 2005. Detailed spatially distributed geothermal heat-flow data for modeling of basal temperatures and meltwater production beneath the Fennoscandian ice sheet. Annals of Glaciology 40, 95–101.

Paterson W S B, 1994. The physics of glaciers. 3rd ed. Oxford: Pergamon.

Piotrowski J A, 2006. Groundwater under ice sheets and glaciers. In Knight P G (ed). Glacier science and environmental change. Malden, MA: Blackwell, 50–60.

Pusch R, Börgesson L, Knutsson S, 1990. Origin of silty fracture fillings in crystalline bedrock. Geologiska Föreningen i Stockholm Förhandlingar 112, 209–213.

Ramana Y V, Gogte B S, 1989. Dependence of coefficient of sliding friction in rocks on lithology and mineral characteristics. Engineering Geology 26, 271–279.

Rapp A, 1996. Impact of mountain glaciations on tors, blockfields and cryoplanation features. Nunataks or non-scoured zones as refugia? In McCann S B, Ford D C (eds). Geomorphology Sans Frontières. Chichester: Wiley, 137–152.

Rastas J, Seppälä M, 1981. Rock jointing and abrasion forms on *roches moutonnées*, SW Finland. Annals of Glaciology 2, 159–163.

Ruszcyńska-Szenajch H, 1987. The origin of glacial rafts: detachment, transport, deposition. Boreas 16, Issue 2, 101–112.

Ryser C, Lüthi M P, Andrews L C, Hoffman M J, Catania G A, Hawley R L, Neumann T A, Kristensen S S, 2014. Sustained high basal motion of the Greenland ice sheet revealed by borehole deformation. Journal of Glaciology 60, 647–660.

SKB, 2010. Climate and climate-related issues for the safety assessment SR-Site. SKB TR-10-49, Svensk Kärnbränslehantering AB.

Talbot C J, 1999. Ice ages and nuclear waste isolation. Engineering Geology 52, 177–192.

Talbot C J, 2014. Comment on "Approach to estimating the maximum depth for glacially induced hydraulic jacking in fractured crystalline rock at Forsmark, Sweden" by M. Lönnqvist and H. Hökmark. Journal of Geophysical Research: Earth Surface 119, 951–954.

Waller R I, Murton J B, Kristensen L, 2012. Glacier-permafrost interactions: Processes, products and glaciological implications. Sedimentary Geology 255, 1–28.

Zoet L K, Carpenter B, Scuderi M, Alley R B, Anandakrishnan S, Marone C, Jackson M, 2013. The effects of entrained debris on the basal sliding stability of a glacier. Journal of Geophysical Research: Earth Surface 118, 656–666.

Appendix 1

Constants, parameters with chosen values, and variables

Constant / parameter	Symbol	Value
density of ice	ρ_i	910 kg m^{-3}
density of water	ρ_w	1 000 kg m^{-3}
density of rock	ρ_r	2 800 kg m^{-3}
standard acceleration of gravity	g	9.8 m s^{-2}
year	yr	3.15×10^7 s
geothermal heat flow	Q_{geo}	30–85 mW m^{-2}
heat of fusion ice	H_{ice}	334 kJ kg^{-1}

Variable	Symbol	Unit
ice thickness	h_i	m
length of block	L	m
height of block	H	m
width of block	W	m
surface area top of block	A	m^2
radius of sphere	r	m
rock-rock friction coefficient	μ_{rr}	-
ice-rock friction coefficient	μ_{ir}	-
normal force acting vertically on basal plane	F_z	N
horizontal resisting force	F_{rx}	N
buoyant weight of block	F_{bz}	N
weight overlying ice	F_{iz}	N
drag force by downward ice flow	F_{mz}	N
horizontal driving force	F_{dx}	N
horizontal shear stress	τ_{dx}	Pa
cryostatic pressure	P_i	Pa
water pressure	P_w	Pa
relative effective pressure	P_{ref}	0–1
sliding velocity at base	U_{sl}	m s^{-1} or m yr^{-1}
vertical velocity of ice around block	U_{mz}	m s^{-1} or m yr^{-1}

Appendix 2

Reynolds number and ice flow

The Reynolds number is a dimensionless number, given by:

$$R_e = {}^{\rho UL}/_{\eta} \qquad \text{(A2-1)}$$

where ρ is the density of the fluid, U is the velocity of the fluid, L a characteristic length for instance the size of an obstacle or the width of channel, and η the viscosity of the fluid (e.g. Furbish 1997). The Reynolds number can be seen to determine whether a fluid flow is laminar or turbulent, with laminar flow occurring if Re < 1, and turbulent flow if Re > 2 000, with a transitional regime in between these values.

Ice flow in general has Re << 1, and can thus be regarded as laminar. As an example, for temperate ice with $\eta = 1.3 \times 10^{11}$ Pa s (after Byers et al. 2012), with $U = 1.1 \times 10^{-3}$ m s^{-1} (~ 100 m day^{-1}) and an obstacle size $L = 10$ m, Re ~ 7.7×10^{-11}. Although ice velocity and ice viscosity can vary by two orders of magnitude, it is clear that ice falls well and truly in the laminar regime. Water, by contrast, is in all but the smallest tube (i.e. veins) turbulent. For example, with $\eta = 1.8 \times 10^{-3}$ Pa s (at 0 °C, after Engineeringtoolbox.com), with $U = 1$ m s^{-1} and an obstacle size $L = 1$ m, the Reynold's number Re ~ 5.5×10^{5}, well and truly in the turbulent regime.

Arkitektkopia AB, Bromma, 2019

SKB is responsible for managing spent nuclear fuel and radioactive waste produced by the Swedish nuclear power plants such that man and the environment are protected in the near and distant future.

skb.se